JCI insight

# β-Catenin Stabilization Protects Against Alveolar Hemorrhage Through Amphiregulin and BATF-Mediated Regulatory T Cells

Fiona Mason, Hui Xiong, Ali Mobeen, Md Saddam Hossain, Sara Mahmudlu, Rosanne Trevail, Mikyal Mobeen, Li Chen, Sunny Lee, Tuncay Delibasi, Jyoti Misra Sen, Mobin Karimi

*JCI Insight*. 2026. https://doi.org/10.1172/jci.insight.201552.

**Research** In-Press Preview **Immunology**

## Graphical abstract

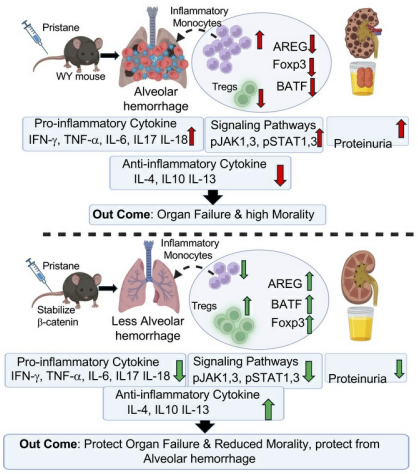


## Find the latest version:

https://jci.me/201552/pdf

# β-Catenin Stabilization Protects Against Alveolar Hemorrhage Through Amphiregulin and BATF-Mediated Regulatory T Cells

Fiona Mason[1], Hui, Xiong[2], Ali Mobeen[1], Md Saddam Hossain[1], Sara Mahmudlu[1], Rosanne Trevail[1], Mikyal Mobeen[1], Li Chen[3], Sunny Lee[1], Tuncay Delibasi[4], Jyoti Misra Sen[5,6], and Mobin Karimi[1]

[1]Department of Microbiology and Immunology, SUNY Upstate Medical University, Syracuse, NY 13210.
[2]School of Medical Imaging, Nanchang Medical College, Nanchang, Jiangxi, China.
[3]Department of Pathology, SUNY Upstate Medical University, Syracuse, NY 13210.
[4]Department of Medicine/ Endocrinology, SUNY Upstate Medical University, Syracuse, NY 13210
[5,] National Institute on Aging, NIH, and [6] Center on Aging and Immune Remodeling Immunology Program Department of Medicine Johns Hopkins University Baltimore, MD 21224

**Authorship notes:** Fiona Mason, Hui, Xiong contributed equally to this work.

**Conflict of interest:** The authors have declared that no conflict of interest exists.



Key Words:

- β-Catenin Stabilization
- Alveolar Hemorrhage
- Amphiregulin, Transcriptional Factor BATF
- Regulatory T cells.
- Inflammatory Monocytes

Abstract words 199
Total word count: 10, 970

Abstract

Alveolar hemorrhage (AH) is a life-threatening condition with high mortality, yet the immunologic mechanisms governing disease severity remain poorly defined. Here, we demonstrate a protective role for T cell–intrinsic β-catenin stabilization in AH using a transgenic mouse model (CAT-Tg) in which β-catenin is stabilized under the Lck promoter. β-Catenin stabilization induced a distinct T cell phenotype marked by expansion of central effector memory cells ($CD44^+CD122^+Eomes^+T\text{-}bet^+$) and suppression of proinflammatory signaling, including reduced phosphorylation of STAT1, STAT3, and JAK1. Pristane-induced AH was attenuated in CAT-Tg mice, which exhibited reduced lung injury, decreased proteinuria, and diminished pulmonary proinflammatory cytokine production compared with wild-type controls. Protection was associated with a marked expansion of $FOXP3^+$ regulatory T cells (Tregs).

Mechanistically, β-catenin stabilization enhanced lung expression of Amphiregulin and BATF, mediators of Treg stability and tissue repair. Adoptive transfer of CAT-Tg–derived Tregs into wild-type mice conferred superior protection against AH, reducing lung inflammation and proteinuria. Transcriptomic analyses revealed enrichment of tissue repair and immune homeostasis pathways, including PI3K–Akt, angiogenesis, and STAT5 signaling. Collectively, these findings identify β-catenin as a regulator of a protective Amphiregulin–BATF–Treg axis, highlighting a immunomodulatory pathway with therapeutic potential for AH and inflammatory lung disease.

## Introduction

Alveolar hemorrhage (AH) is a life-threatening syndrome characterized by bleeding into the alveolar airspaces resulting from immune-mediated injury to the pulmonary microvasculature. It most commonly occurs in autoimmune diseases such as Goodpasture syndrome, systemic lupus erythematosus (SLE), and antiphospholipid syndrome, where immune-mediated capillary damage precipitates pulmonary bleeding (1-3). Current treatment strategies rely on high-dose corticosteroids combined with systemic immunosuppression, including cyclophosphamide, rituximab, and antifibrinolytic agents to stabilize clot formation (3, 4). Despite aggressive therapy, mortality remains unacceptably high, underscoring a critical gap in understanding the immune mechanisms that drive tissue injury versus protection in AH (5-8).

Defining the immune pathways that govern tissue injury and repair in AH is the central objective of this study. Amphiregulin (AREG) and the transcription factor Basic Leucine Catenin (BATF) is a critical upstream regulator of AREG, as canonical β-catenin signaling directly controls its transcription (16, 17). More broadly, β-catenin signaling is essential for T cell development and tissue homeostasis (18). Upon activation, β-catenin translocates to the nucleus and associates with T cell factor/lymphoid enhancer factor (Tcf/Lef) transcription factors to induce target gene expression, including AREG (16, 19). In addition, β-catenin–dependent transcriptional programs support proliferation, migration, and stem cell maintenance during tissue repair (18, 20). In parallel, BATF, a component of the AP-1 transcription factor complex, is essential for the differentiation and function of multiple immune cell subsets, including T cells and innate lymphoid cells (ILCs) (21, 22). Regulatory T cells ($FOXP3^+$ Tregs) represent another critical axis of

64 immune tolerance and tissue repair, and AREG has been shown to enhance Treg suppressive function (10, 23). Despite these established
65 roles, the upstream molecular pathways that integrate β-catenin signaling with BATF and AREG regulation in Tregs remain undefined

66 Here, we show that β-catenin regulates FOXP3 expression and enhances BATF- and AREG–dependent Treg function, thereby
67 conferring protection against AH. Using transgenic mice with stabilized β-catenin under the lymphocytes Specific Protein Tyrosine
68 Kinase (Lck) promoter (CAT-Tg) (24-26), we found that CAT-Tg $CD8^+$ T cells exhibit expanded central memory (CM) and effector
69 memory (EM) subsets, increased expression of CD44, CD122, T-box transcription factors Eomesodermin (Eomes) and T-box
70 transcription factors (T-bet) and reduced phosphorylation of Signal Transducer and Activator of Transcription 1 (STAT1), STAT3, and
71 Janus Kinase 1 (JAK1). Consistent with these immunologic changes, CAT-Tg mice were protected from pristane-induced AH,
72 displaying attenuated lung pathology, reduced proteinuria, diminished proinflammatory cytokine production, and enhanced anti-
73 inflammatory responses compared with wild-type (WT) controls. Importantly, this protection was associated with increased frequencies
74 of $FOXP3^+$ Tregs expressing high levels of AREG and BATF.

75 Adoptive transfer of CAT-Tg Tregs into WT recipients with pristane-induced AH conferred robust protection, reducing lung
76 inflammation and proinflammatory cytokine production while enhancing anti-inflammatory cytokines expression. Consistently,
77 pharmacologic activation of β-catenin in WT mice protected against AH, suppressing inflammatory cytokines and expanding Treg
78 populations. Unbiased RNA sequencing further revealed that β-catenin stabilization reprograms gene expression toward tissue repair
79 and immune homeostasis. Collectively, these findings identify a previously unrecognized β-catenin–AREG–BATF–Treg axis that

protects against alveolar hemorrhage. This work defines β-catenin as a therapeutic target for AH and other cytokine storm–mediated inflammatory lung diseases.

## Results

**β-Catenin stabilization alters the CD8$^+$ T cell phenotype:** β-Catenin is required for both alpha beta (αβ) and gamma delta (γδ) T cell development (27-29). To determine whether stabilization of β-catenin under the Lck promoter (Cat-Tg mice) (30, 31)**,** alters αβ T cell differentiation, we analyzed T cell subsets in WT and CAT-Tg mice both in C57BL/6 (B6) background. Because αβ T cell phenotype reflects differentiation status, effector function, and persistence relevant to therapeutic efficacy (32-35), freshly isolated splenic CD3$^+$ T cells were analyzed by flow cytometry. Cells were gated on total T cells and subdivided into CD4$^+$ and CD8$^+$ populations, which were further classified as naïve, CM, or EM subsets based on CD44 and CD62L expression (36, 37). CD62L mediates homing to secondary lymphoid tissues, whereas CD44 is associated with activation and migration to peripheral or inflamed sites (38-41). CAT-Tg mice exhibited a significantly increased proportion of CM and EM CD8$^+$ T cells compared with WT controls (Fig. 1A–E). In contrast, the distribution of naïve, CM, and EM subsets within the CD4$^+$ T cell compartment was unchanged between CAT-Tg and WT mice (Fig. 1F–J). These findings indicate that β-catenin stabilization preferentially drives memory differentiation in CD8$^+$ T cells, a subset critical for long-term antitumor immunity.

**CD8$^+$ T cells from CAT-Tg mice display increased activation markers with attenuated signaling:** We previously showed that T cells with attenuated T cells receptor signaling can exhibit elevated activation markers without inducing alloimmunity (31, 36, 42-44). Consistent with this, flow cytometric analysis revealed significantly increased CD44 expression on CD3$^+$CD8$^+$ T cells from CAT-Tg mice compared with WT controls, as demonstrated by representative plots and quantitative analyses (Fig. 2A–B). We next examined

transcriptional regulators of $CD8^+$ T cell memory differentiation. The T-bet and Eomes cooperatively promote memory formation by inducing CD122, a critical component of Interleukin-2 (IL-2) and interleukin -15 (IL-15) signaling (45, 46). In line with enhanced memory potential, $CD8^+$ T cells from CAT-Tg mice expressed significantly higher levels of T-bet, Eomes, and CD122 than WT $CD8^+$ T cells (Fig. 2C–H).

Finally, we examined whether β-catenin stabilization alters proximal T cell signaling. STAT1, STAT3, and JAK1 are central components of the JAK–STAT pathway that regulate T cell growth, differentiation, and immune responses (47, 48). Following CD3/CD28 stimulation, CAT-Tg T cells exhibited reduced phosphorylation of STAT1, STAT3, and JAK1 compared with WT controls (Fig. 2I). These findings indicate that β-catenin stabilization promotes a highly activated, memory-prone $CD8^+$ T cell phenotype while concurrently attenuating JAK–STAT signaling. β-catenin stabilization markedly reduced severe inflammatory autoimmunity, including AH, bronchiectasis, and related autoimmune manifestations (48).

**β-Catenin stabilization protects mice from AH:** To determine whether β-catenin stabilization exacerbates or ameliorates AH, 6–8-week-old WT and CAT-Tg mice were analyzed. Baseline urine and serum samples were collected prior to intraperitoneal (IP) injection of pristane (0.5 mL per 20 g body weight) to induce AH (32, 49, 50). Mice were monitored daily for weight loss and clinical signs of disease; no significant weight loss was observed over the 14-day experimental period. On day 14, mice were euthanized and lungs were harvested (Fig. 3A). Gross examination revealed marked protection from AH in CAT-Tg mice compared with WT controls (Fig. 3B–E). Histological analysis of lung sections stained with hematoxylin and eosin (H&E) confirmed reduced AH in CAT-Tg mice. All lung

sections were independently evaluated by a blinded pathologist, and double-blind pathological scoring validated the protective effect of β-catenin stabilization (Fig. 3F). Additional organs, including kidney, liver, and spleen, showed no significant differences between WT and CAT-Tg mice at the 14-day time point (Supplemental Fig. 1A–O). In contrast, significant pathological differences were observed in these organs at 3 months (data not shown).

To characterize immune cell infiltration during AH (51), pristane-induced AH was established in WT and CAT-Tg mice. 14 days after pristane injection, lungs were harvested; one cohort was processed for flow cytometric analysis, and a second cohort was prepared for immunohistochemistry (IHC). Because inflammatory monocytes are known contributors to lung injury in AH lung leukocytes were analyzed for CD11b and Ly6C expression (52-54). Lungs from WT mice contained a high frequency (80%–90%) of $CD11b^{+}Ly6C^{+}$hi inflammatory monocytes. In contrast, $CD11b^{+}$ monocytes from CAT-Tg mice expressed significantly lower levels of Ly6C, indicating reduced inflammatory infiltration (Fig. 3G). Consistent with these findings, IHC analysis confirmed the presence of $CD11b^{+}Ly6C^{+}$ infiltrates within lung tissue (Fig. 3H), with representative images showing DAPI (blue), Ly6C (red), and CD11b (green). Together, these data establish pristane-induced AH as a highly inflammatory model and demonstrate that β-catenin stabilization markedly attenuates inflammatory monocyte accumulation in the lung. Having established a protective effect of β-catenin stabilization, we next investigated the immunological mechanisms underlying this protection.

**β-Catenin stabilization reduces proteinuria and suppresses proinflammatory cytokines during AH:** Proteinuria, a hallmark of pulmonary–renal syndrome, frequently accompanies AH in systemic autoimmune disease and serves as an early indicator of kidney

involvement (55). To assess renal injury, proteinuria was measured by ELISA in WT and CAT-Tg mice before and after pristane-induced AH. WT mice exhibited a significant increase in proteinuria by day 14 post-pristane injection compared with baseline levels. In contrast, CAT-Tg mice showed no significant change in proteinuria following pristane treatment, indicating that β-catenin stabilization protects against AH-associated renal injury (Fig. 4A–C). Given that pristane-induced AH is characterized by robust inflammatory responses (Fig. 3), we next evaluated circulating proinflammatory cytokines. Interferon-γ (IFN-γ) and tumor necrosis factor–α (TNF-α) are key mediators of AH pathogenesis, acting synergistically to promote tissue factor expression and procoagulant activity (56). WT mice displayed significant increases in both IFN-γ and TNF-α at day 14 post-pristane injection, whereas CAT-Tg mice exhibited no significant changes in these cytokines relative to baseline (Fig. 4D–E). Because IL-6 and IL-18 are key mediators of lung injury and hemorrhage (57, 58), we next assessed their serum levels. IL-6 promotes neutrophil recruitment, a hallmark of hemorrhagic inflammation, whereas IL-18 amplifies inflammasome-driven cascades that increase vascular permeability and alveolar bleeding. Following AH induction, CAT-Tg mice exhibited significantly lower levels of both IL-6 and IL-18 compared with WT controls (Fig. 4F–H). IL-17 has also been implicated in lung injury, edema, and AH (59-61); consistent with a protective phenotype, CAT-Tg mice displayed markedly reduced IL-17 induction relative to WT mice (Fig. 4G). IL-5 shows increase production in CAT-Tg mice at day 14 post pristane-induced AH (Fig. 4J). We next examined whether β-catenin stabilization enhances anti-inflammatory cytokine production. Serum from CAT-Tg mice contained significantly higher levels of IL-4, IL-13, and IL-10 compared with WT mice (Fig. 4J–L). In contrast, IL-12 and IL-9 levels were not significantly different between groups (Supplemental Fig. 2), indicating selective modulation of anti-inflammatory pathways (62, 63). These data demonstrate that β-catenin stabilization protects against AH by

concurrently suppressing proinflammatory cytokines (IFN-γ, TNF-α, IL-6, IL-18, and IL-17) and enhancing anti-inflammatory cytokines (IL-4, IL-13, and IL-10). Having established both structural and cytokine-level protection, we next investigated the mechanistic basis by which β-catenin attenuates AH severity.

**β-Catenin stabilization enhances amphiregulin, and BATF expression in Tregs:** The role of Tregs in ameliorating AH has not been well defined. Tregs are established mediators of immune suppression and tissue repair, acting through the release of anti-inflammatory cytokines such as interleukin 10 (IL-10) to limit neutrophil and inflammatory monocyte activity, and by restoring immune balance following injury (64, 65). In addition, Tregs directly promote tissue repair after inflammatory damage (64, 66). To determine whether β-catenin stabilization affects Tregs, splenocytes and lung from WT and CAT-Tg mice were analyzed by flow cytometry. $CD3^+CD4^+$ T cells were gated and assessed for CD25 and FOXP3 expression. CAT-Tg mice exhibited a significantly increased frequency of Tregs, including both conventional $CD25^+FOXP3^+$ and non-canonical $CD25^-FOXP3^+$ subsets (67, 68), compared with WT controls (Fig. 5A–E). These data suggest that β-catenin stabilization promotes Treg expansion during AH. To further define Treg-mediated protective mechanisms, we examined Areg, an epidermal growth factor receptor ligand that promotes tissue repair independently of classical Treg suppressive functions (23, 69-71). $CD25^+FOXP3^+$ Tregs were FACS-sorted from the lungs of WT and CAT-Tg mice using FOXP3–RFP reporter expression (Fig. 5C–D), and Areg expression was assessed by immunoblotting. Tregs from CAT-Tg mice expressed substantially higher levels of Areg than WT controls (Fig. 5F), indicating enhanced tissue-repair capacity. Consistent with this phenotype, CAT-Tg Tregs also expressed significantly higher levels of the transcription factor BATF, which is

required for Treg homeostasis, differentiation, and stability (15). (Fig. 5F). BATF sustains FOXP3 expression, these findings indicate that β-catenin stabilization not only expands Treg populations but also reinforces their lineage stability and suppressive function, thereby limiting uncontrolled inflammation. Collectively, these results demonstrate that β-catenin stabilization programs a protective, lineage-stable Treg phenotype with enhanced expansion and tissue-repair capacity. We next tested the functional consequences of CAT-Tg–derived Tregs in vivo.

**Adoptive transfer of CAT-Tg Tregs rescues AH in vivo**: To determine whether Tregs from CAT-Tg mice, characterized by elevated Areg and BATF expression, confer protection against AH in vivo, we performed adoptive transfer experiments. WT mice were divided into three groups: untreated controls, recipients of WT Tregs, and recipients of CAT-Tg Tregs. Baseline serum and urine samples were collected prior to pristane administration. AH was induced by pristane injection, and disease was allowed to establish for 10 days. At day 10 post-pristane injection, splenic $CD3^+CD4^+CD25^+FOXP3^+$ Tregs were FACS-purified from WT or CAT-Tg donor mice and adoptively transferred ($1 \times 10^6$ cells per mouse) into WT recipients, while one cohort remained untreated. At day 21 post-pristane injection, lungs, serum, and urine were collected for analysis (Fig. 6A–D). Gross pathological examination revealed severe AH in untreated pristane-injected WT mice (Fig. 6D). In contrast, mice receiving Tregs from CAT-Tg mice were fully protected, with lungs appearing grossly normal, whereas recipients of WT Tregs exhibited only partial protection. Consistent with lung pathology, proteinuria was markedly elevated in untreated and WT Treg–recipient mice compared with baseline levels, while adoptive transfer of CAT-Tg Tregs completely prevented proteinuria (Fig. 6E–G). Together, these findings demonstrate that CAT-Tg Tregs confer superior protection

against both pulmonary and renal injury during AH. Cytokine analyses further demonstrated the superior protective capacity of CAT-Tg Tregs. WT mice receiving CAT-Tg Tregs exhibited significantly reduced levels of IFN-γ and TNF-α compared with mice receiving WT Tregs (Fig. 6H–I). IL-17 levels were unchanged in CAT-Tg Treg recipients, whereas WT Tregs only modestly reduced IL-17 relative to untreated mice and remained significantly higher than levels observed in CAT-Tg Treg recipients (Fig. 6J). Importantly, adoptive transfer of CAT-Tg Tregs induced a robust increase in IL-10, a key anti-inflammatory cytokine, compared with both untreated and WT Treg–treated mice (Fig. 6K). Together, these findings indicate that β-catenin stabilization enhances Treg-mediated protection against AH by suppressing proinflammatory cytokines while promoting IL-10 production.

To assess the persistence and tissue trafficking of donor Tregs, adoptive transfer experiments were repeated using congenic CD45.2 WT recipients and CD45.1 donor mice. At day 21 post-transfer, both donor- and host-derived Tregs were detected in the spleen (Supplemental Fig. 3A–C). IHC analysis of lung tissue identified donor Tregs within inflamed lungs, confirmed by colocalization of CD4 (green), donor CD45.1 (blue), and FOXP3 (red) signals (Supplemental Fig. 3D–J). These data confirm engraftment and lung homing of donor CAT-Tg Tregs. Collectively, these results demonstrate that CAT-Tg Tregs, enriched for AREG and BATF, confer superior protection against AH compared with WT Tregs by suppressing proinflammatory cytokines, enhancing IL-10 production, and efficiently trafficking to sites of lung inflammation.

**β-Catenin agonists recapitulate the protective effects of genetic stabilization:** To determine whether pharmacologic activation of β-catenin can mimic genetic stabilization in vivo, we treated WT mice with Wnt/β-catenin agonists (MedChemExpress; HY-114321) (72-

74), in a pristane-induced AH model. WT mice were injected with pristane, and urine and blood were collected for baseline and post-treatment analyses. Mice received either vehicle (DMSO) or a β-catenin agonist (10 μg per 20 g body weight) twice weekly for 14 days (Fig. 7A–B). Animals were euthanized on day 14, and lungs were harvested for analysis. Treatment with β-catenin agonists significantly increased the frequency of $FOXP3^+$ Tregs in the lungs compared with vehicle-treated controls (Fig. 7C–D). As expected, pristane-injected WT mice exhibited severe lung injury relative to untreated controls, with extensive AH confirmed by H&E staining (Fig. 7D–H). In contrast, WT mice treated with the β-catenin agonist showed minimal lung damage despite pristane challenge, whereas vehicle-treated mice displayed substantial hemorrhage (Fig. 7I–J). Quantitative assessment demonstrated significantly reduced red blood cell accumulation and tissue injury in the β-catenin agonist–treated group (Fig. 7K–M). Collectively, these findings demonstrate that pharmacologic activation of β-catenin phenocopies genetic stabilization, protecting against pristane-induced AH by promoting a suppressive, Treg-mediated immune program.

**β-Catenin agonists reduce proteinuria and proinflammatory cytokines in the AH model:** To determine whether pharmacologic β-catenin activation suppresses inflammatory responses during AH), AH was induced as described above (Fig. 7–8A). Urine analysis revealed that WT mice injected with pristane and treated with vehicle developed significantly increased proteinuria compared with pre–pristane baseline levels. In contrast, WT mice treated with β-catenin agonists exhibited no significant change in proteinuria before versus after pristane injection, indicating protection from renal injury (Fig. 8B–C). Consistent with these findings, β-catenin agonist–treated mice displayed significantly reduced serum levels of IFN-γ and TNF-α compared with untreated or vehicle-treated controls. However,

cytokine suppression was incomplete and did not reach the magnitude observed with genetic β-catenin stabilization (Fig. 8D–E). Similarly, levels of IL-6 and IL-17 were reduced following β-catenin agonist treatment, albeit to a lesser extent than in the genetic model (Fig. 8F–G). Notably, β-catenin agonist treatment significantly increased IL-10 production relative to untreated and vehicle-treated controls (Fig. 8H). In contrast, no significant differences were observed in IL-12 or IL-13 levels (Supplemental Fig. 4). These data showed that pharmacologic β-catenin activation amplifies Treg-associated anti-inflammatory responses while suppressing proinflammatory cytokine production, supporting its therapeutic potential for AH.

**β-Catenin stabilization regulates gene expression during AH:** Our findings demonstrate that β-catenin stabilization protects the lung from AH and promotes expansion of Tregs expressing Areg and BATF, which contribute to tissue repair and suppression of inflammatory cytokines. However, the global transcriptomic programs regulated by β-catenin stabilization during AH remained undefined. To address this, AH was induced with pristane as described above, and lung tissues were harvested at day 14 for bulk RNA sequencing. Principal component analysis (PCA) revealed clear segregation between WT and CAT-Tg samples (PC1: 53.05%, PC2: 25.60%, PC3: 12.05%) (Fig. 9A). Differential expression analysis identified 2,688 genes (FDR $\leq 0.05$, $|\log_2 FC| \geq 0.5$), with 1,464 genes downregulated and 1,224 genes upregulated in CAT-Tg lungs compared with WT controls (Fig. 9B). Hierarchical clustering of normalized expression values separated these genes into two modules: Module 1, comprising genes downregulated in CAT-Tg samples, and Module 2, comprising genes upregulated in CAT-Tg samples (Fig. 9C). Gene Ontology analysis of Module 1 revealed enrichment of pathways related to stress responses, immune activation, and inflammation. In contrast, Module 2 was enriched for pathways

associated with cell projection assembly, cell motility, and tissue organization. Gene set enrichment analysis using Hallmark pathways from MSigDB (74) demonstrated broad enrichment of inflammatory, stress-response, metabolic, and cell-cycle pathways—including TNFα– Nuclear Factor kappa-light-chain-enhancer (NF-κB), IL6–JAK–STAT3, IFN-γ response, oxidative stress, coagulation, and hypoxia—in WT lungs relative to CAT-Tg samples (Fig. 9D–H). Conversely, Kirsten rat sarcoma virus oncogene homolog (KRAS) signaling (down) was selectively enriched in CAT-Tg lungs. Collectively, these data demonstrate that β-catenin stabilization rewires lung transcriptional programs during AH, suppressing inflammatory and stress-response pathways while activating cell motility and tissue-repair programs, thereby establishing a protective and regenerative immune environment.

**β-Catenin agonists impact gene expression during AH:** To determine whether pharmacologic β-catenin activation recapitulates the transcriptomic effects of genetic stabilization during AH, WT mice were subjected to pristane-induced AH and treated with either vehicle or a β-catenin agonist, as described above. At day 14, lungs were harvested for bulk RNA sequencing. Differential expression analysis identified 2,565 genes (FDR $\leq 0.05$, $|\log_2 FC| \geq 0.5$) between agonist- and vehicle-treated lungs, with 1,583 genes downregulated and 982 genes upregulated in agonist-treated samples (Fig. 10B). Principal component analysis demonstrated clear separation between agonist- and vehicle-treated groups (PC1: 65.84%, PC2: 20.22%, PC3: 6.82%) (Fig. 10A). Gene Ontology enrichment analysis of downregulated genes (Module 1) revealed pathways associated with immune activation, stress responses, and proliferative signaling, including BCR stimulation, immune system processes, E2F-associated complexes, and cell-cycle–related pathways. In contrast, upregulated genes (Module 2) were enriched for pathways related to cell projection assembly, microtubule organization, cilium-

dependent motility, and cytoskeletal remodeling. Gene set enrichment analysis using Hallmark pathways demonstrated significant negative enrichment of inflammatory, stress-response, and proliferative programs in agonist-treated lungs, including IFN-γ response, TNFα–NF-κB signaling, IL6–JAK–STAT3 signaling, Transcription factors E2F targets, G2M checkpoint, Mechanistic Target of Rapamycin Complex 1 (mTORC1) signaling, epithelial–mesenchymal transition, and oxidative phosphorylation (Fig. 10C–G). These findings shows that pharmacologic β-catenin activation recapitulates the transcriptomic reprogramming observed with genetic stabilization by suppressing inflammatory and stress-response pathways while enhancing motility- and repair-associated programs, supporting a mechanistic basis for therapeutic protection during AH.

## Discussion

Alveolar hemorrhage (AH) is a life-threatening condition marked by severe pulmonary inflammation and high mortality (75-79). Despite its clinical impact, the immunological mechanisms by which Tregs mitigate lung injury in AH remain incompletely defined. We previously showed that T cells from CAT-Tg mice mediate potent antitumor immunity without inducing graft-versus-host disease (GVHD) in an allogeneic transplant model (42). In that context, CAT-Tg T cells displayed an activated phenotype characterized by expanded CM and EM memory subsets and increased expression of CD44, CD122, Eomes, and T-bet (Fig. 1–2).

In this study, we show that stabilization of β-catenin under the proximal Lck promoter (29) recapitulates and extends these immunologic features in inflammatory lung injury. β-Catenin stabilization expanded Tregs, resembling the phenotype of T cells with attenuated TCR signaling—an immune-regulatory state rather than a pathogenic one. While β-catenin has been implicated in thymocyte development (29), our data extend this role to the periphery, establishing β-catenin as a regulator of T cell activation, lineage stability, and tissue-protective function.

Using a pristane-induced murine AH model, we show that constitutive β-catenin expression confers robust protection against lung injury. CAT-Tg mice displayed markedly reduced hemorrhage and preserved lung architecture compared with WT controls. No significant differences were observed in liver, kidney, or spleen pathology within the first 14 days, suggesting an early, lung-focused protective effect. However, wild-type mice developed early proteinuria and later renal and splenic pathology (4–6 weeks), indicating that β-catenin signaling may also influence systemic disease progression over time. Our data show that β-catenin stabilization reduces phosphorylation of STAT1, STAT3, and JAK1—central nodes in cytokine signaling downstream of IFN-γ, IL-6, TNF-α, IL-18, IL-17,

and IL-4 (48, 68). Consistent with this signaling restraint, CAT-Tg mice exhibited markedly lower proinflammatory cytokines (IFN-γ, IL-6, TNF-α, IL-18, IL-17, and IL-5) during AH, alongside increased anti-inflammatory cytokines including IL-4, IL-13, and IL-10 (80, 81). Collectively, these findings position β-catenin as a key regulator of cytokine storm severity and a potential therapeutic target for AH and other cytokine-driven inflammatory diseases.

Tregs are central to immune homeostasis and help suppress inflammation and cytokine storm–driven pathology (36, 82). However, induced Tregs often lose FOXP3 expression and lineage stability during in vitro expansion (83, 84), whereas naturally occurring Tregs are present at low frequencies in vivo. Notably, CAT-Tg mice exhibited a marked expansion of Tregs relative to WT controls, with increased accumulation in the lung during AH (Fig. 5A–E). To define the mechanisms underlying this protective response, we focused on AREG and the transcription factor BATF, key regulators of tissue repair and immune stability (9-15). β-Catenin stabilization activates transcriptional programs that include direct induction of AREG (16, 19); consistent with this, CAT-Tg lungs expressed elevated AREG levels and were protected from AH (18, 20). Functional relevance was supported by adoptive transfer experiments in which CAT-Tg–derived Tregs conferred robust protection, suppressing IFN-γ, TNF-α, and IL-17 while enhancing IL-10 production (Fig. 6). Collectively, these findings link β-catenin stabilization to Treg expansion and stability and to tissue repair during AH. Because genetic models are not always directly translatable, we next evaluated pharmacologic strategies to activate β-catenin during AH. Treatment of WT mice with β-catenin agonists increased Treg frequencies, reduced proinflammatory cytokine production, and enhanced IL-10 expression, conferring significant protection against AH. Pharmacologic β-catenin activation largely recapitulated the protective effects of genetic β-catenin stabilization. These findings support therapeutic targeting of β-catenin in AH and potentially other

cytokine storm–mediated inflammatory diseases. RNA-sequencing analyses show that β-catenin stabilization reprograms lung transcriptional landscapes during AH by suppressing inflammatory and stress-response pathways while activating cell motility and tissue-repair programs, thereby promoting a protective, regenerative environment. Pharmacologic β-catenin activation closely mirrored these transcriptomic effects, attenuating inflammatory, stress-response, and proliferative signaling while enhancing ciliary and motility-associated pathways. Collectively, these findings establish β-catenin stabilization as a central regulator of protective transcriptional programs during AH, with therapeutic potential to suppress inflammation and promote tissue repair.

## Materials and Methods

### Mice

Sex as a biological variable, we used both male and female mice. However, female did not show serve AH. Mice in these studies were used all male. CAT-Tg mice have been previously described (30, 31) and were generously provided by Dr. Jyoti Misra Sen (National Institute on Aging, NIH). C57BL/6 mice were purchased from Charles River Laboratories or The Jackson Laboratory. Mice aged 8–12 weeks were used for all experiments, with age- and sex-matched controls included throughout.

### Reagents, cell lines, flow cytometry

Monoclonal antibodies were purchased from BioLegend or eBioscience and BD Pharmingen. All flow cytometry antibodies were used at a 1:100 dilution unless otherwise indicated. Antibodies included anti-mouse CD3 (Cat# 100102), anti-CD28 (Cat# 102116), CD3-BV605 (Cat# 100237), CD4-PE (Cat# 100408), CD8-PE/Cy7(Cat# 100722), Eomes-PE/Cy7 (Cat# 25-4877-42), CD44–Pacific Blue (Cat# 156006), CD122-APC (Cat# 105912), CD62L-APC/Cy7(Cat# 304814), T-bet–BV421(Cat# 644816), TNF-α–FITC (Cat# 502906), IFN-γ–APC (Cat# 505810), TCF-1–PE (Cat# 564217), FOXP3–Pacific Blue (Cat# 126410), CD25–FITC(Cat# 101908), CD11b- FITC (Cat# 101205), and Ly-6C- APC (Cat# 128016). Flow cytometry was performed on a BD LSRFortessa (BD Biosciences). Dead cells were excluded using a Live/Dead viability dye (BioLegend), and singlets were identified by forward and side-scatter properties. $CD4^+$ and $CD8^+$ T cells were gated from live $CD3^+$ T cells, and surface and intracellular markers (CD44, CD62L, T-bet,

Eomes, TCF-1, FOXP3, and cytokines) were analyzed within these subsets. Data were analyzed using FlowJo (Tree Star, Ashland, OR) as previously described (67, 68).

**Consumable:** All Consumable were purchased from EIMMUNA Medical supply.

**Proteinuria Assays.**

Urine was collected on day 0 (pre-pristane) and on days 14 or 21 after pristane injection. Total urinary protein was quantified using a BCA Protein assay Kit Cat# 23225) Thermo Scientific (Pierce). Urine was diluted 1:10 in PBS (3 µL urine + 27 µL PBS) and mixed with BCA working reagent (50:1, reagent A: reagent B). Diluted urine (25 µL) was combined with working reagent (200 µL) in a 96-well plate, briefly centrifuged (30 s at 1,250 rpm), and incubated at 37°C for 30 minutes. Absorbance was measured at 562 nm using a BioTek FLx800 plate reader, and protein concentrations (µg/mL) were calculated in Gen5 using a bovine serum albumin (BSA) standard curve.

**Cytokine production, assays.**

Serum was collected from cardiac blood at baseline (pre-pristane) and on day 14 after treatment. Cytokine concentrations—including IFN-γ, TNF-α, IL-5, IL-12, IL-6, IL-10, IL-9, IL-17A, IL-17F, IL-22, IL-13—were quantified using a multiplex bead-based immunoassay (LEGENDplex™, BioLegend) (Cat# 741011 ) according to the manufacturer's instructions (43, 44). Samples were

acquired on a BD LSRFortessa (BD Biosciences), and cytokine concentrations were calculated using LEGENDplex Data Analysis Software (BioLegend).

**Western blotting**

For STAT and JCK signaling T cells were Isolated from either WT or Cat-Tg mice using either CD4 beads (Cat# 130-114-043) or CD8 beads (Cat# 130-117-044) from Miltenyi Biotec, Inc. Cell were stimulated with precoated plates with purified CD3 (Cat# 100202) and CD28 (Cat# 122022) both from bioligand. Cells were stimmed for 5 minutes. For Western data showed in (Fig 5F) Tregs from either WT or CAT-Tg were sorted as described below. Cells in both cases were lysed in freshly prepared RIPA buffer (Fisher Scientific; Cat# PI9900) supplemented with a complete protease inhibitor cocktail (Sigma-Aldrich; Cat# 11697498001) and clarified by centrifugation at 14,000 rpm for 10 minutes at 4°C. Lysates equivalent to $1 \times 10^6$ cells per sample were resolved on 12%–18% SDS–polyacrylamide gels and transferred to nitrocellulose membranes for immunoblotting. Unless otherwise specified, reagents were obtained from Invitrogen (Grand Island, NY) or Sigma-Aldrich (St. Louis, MO). For signaling analyses, membranes were probed with antibodies against phospho-STAT1 (Cell Signaling Technology; Cat# 9167), total STAT1 (Cat# 9172), phospho-STAT3 (Cat# 9131), JAK1 (Cat# 3332), phospho-JAK3 (Cat# 5031), and β-actin (Cat# 4970) (all from Cell Signaling Technology). Additional antibodies included Amphiregulin (AREG; clone AREG559, Thermo Fisher Scientific; Cat# 14-9999-82) and BATF (mouse monoclonal, Thermo Fisher Scientific; Cat# MA5)**.**

**Histopathological evaluation**

Mice were injected with pristane and euthanized on days 14 or 21 post-treatment. Lungs, liver, kidneys, and small intestine were harvested, fixed in 10% neutral-buffered formalin, and processed for paraffin embedding, sectioning, and hematoxylin and eosin (H&E) staining by the Histology Core Facility at SUNY Upstate Medical University. AH pathology was evaluated by a board-certified pathologist (L.C.) blinded to experimental group and disease status. Tissue injury was graded using established criteria (85, 86), and histopathology scores were analyzed using the Mann–Whitney U test.

**Fluorescence microscopy and histologic analysis** Inflammatory monocyte infiltration was assessed 14 days after AH induction in C57BL/6 WT and CAT-Tg mice. Circulating blood was cleared by gentle cardiac perfusion with 2 mL warm PBS using a 25-gauge needle, followed by tracheal inflation with a 1:1 mixture of PBS and O.C.T. compound to preserve alveolar architecture. Lungs were excised, embedded in O.C.T., flash frozen, and cryosectioned at 10 μm. Sections were fixed in acetone (5 minutes, room temperature), blocked for endogenous biotin, and stained overnight at 4°C for $CD11b^{+}$ (Cat# 14-0112-82) Ly6C (Cat# MA1-81899 monocytes. Images were acquired using a Zeiss Axioplan microscope with AxioVision 4.8 software. Histologic scoring was performed by a board-certified pathologist blinded to experimental groups. For IHC, antibodies included anti-CD4 (clone GK1.5, Thermo Fisher Scientific; Cat# 14-0041-82), anti-CD45.2 (; Cat# 14-0454-82), and anti-FOXP3 (Cat# 14-5773-82). Avidin Biotin blocking kit Thermo fisher Scientific (Cat# 001303) Rat IgG2a isotype control Thermo fisher Scientific (Cat# PA533213), Streptavidin Alexa flour 594 Thermo fisher Scientific (Cat# S11227), DAPI (4,6 diamidino 2 phenylindole dihydrochloride (Cat 62247) Thermo fisher Scientific. CD11b mAb

M1/70 Alexa 488, Invitrogen (Cat # 53-0112-80), Ly-6C mAb (Cat# MAI 81899) Invitrogen Secondary Goat anti-Mouse IgG Secondary Antibody, Alexa Fluor 647 (Cat# A32728TR)

**Regulatory T cells (Tregs) isolation**

CAT-Tg and WT mice were bred onto the C57BL/6 background and crossed with the Foxp3tm1Flv/J strain, an X-linked knock-in reporter in which Foxp3-expressing cells are co-marked with monomeric red fluorescent protein (mRFP). In this model, mRFP faithfully reports endogenous Foxp3 expression in lymphocytes. The Foxp3^tm1Flv/J strain was kindly provided by Dr. Avery August (Cornell University), and Foxp3-RFP expression was confirmed in both WT and CAT-Tg mice. $CD4^+$ lymphocytes were isolated from spleens using anti-CD4 magnetic microbeads and column-based separation (Cat# 130-114-043) (Miltenyi Biotec,). Tregs were identified as $CD3^+CD25^+Foxp3(RFP^+)$ cells and purified by fluorescence-activated cell sorting on a BD FACSAria IIIu (BD Biosciences). Sorted Treg purity routinely exceeded 98% unless otherwise specified. Unless noted, reagents and cell culture materials were obtained from Sigma-Aldrich (St. Louis, MO) or Invitrogen (Grand Island, NY), consistent with published protocols (36, 67).

**Statistics.** Data are presented as mean ± SD unless otherwise indicated in the figure legends. Statistical analyses were performed using GraphPad Prism 10. Comparisons were made using unpaired two-tailed Student's *t* test, one- or two-way ANOVA with Tukey's post hoc correction, or chi-square tests, as appropriate. A $P$ value $\leq 0.05$ was considered statistically significant. For in vivo studies, $n = 10$–22 age- and sex-matched mice were used per group, and experiments were independently repeated at least twice. Sample sizes were

based on power calculations unless otherwise specified, and experimental design and matching criteria were consistent with prior studies (24, 31, 36, 37, 42-44, 67, 68, 87-98).

**RNA sequencing**

For genetic β-catenin stabilization studies, four WT and four CAT-Tg mice were injected with pristane and euthanized on day 14. Lungs were harvested and snap frozen. For pharmacologic studies, WT mice were injected with pristane and subsequently treated with a β-catenin agonist as described above, after which lungs were collected. Samples from both studies were processed by the Molecular Analysis Core Facility at SUNY Upstate Medical University for RNA extraction, library preparation, and high-throughput sequencing. RNA-seq datasets included WT, CAT-Tg, and vehicle- versus agonist-treated WT mice following pristane challenge. Data processing and analysis were performed in R (v4.5.1) using RStudio (v2025.05.1+513) and Bioconductor packages. Transcript abundance was quantified by pseudoalignment with Kallisto (v0.51.1) (99), and transcript-per-million (TPM) values were normalized across samples and modeled using the *sleuth* package (100, 101). Differentially expressed genes (DEGs) were defined by $|\log_2 \text{fold change}| \geq 0.5$ and FDR $\leq 0.05$ after Benjamini–Hochberg correction (102). DEG sets were used for hierarchical clustering and heatmap generation in R. Gene Ontology (GO) enrichment was performed using *gprofiler2* (*gost*) (103), and gene set enrichment analysis (GSEA) was conducted using *clusterProfiler* (104), with the MSigDB Hallmark gene sets (105). RNA-seq data have been deposited in the NCBI Gene Expression Omnibus (GEO) database, https://www.ncbi.nlm.nih.gov/geo with the accession number (GSE315191)

**Animal study approval:** All animal housing and experimental procedures were approved by the Institutional Animal Care and Use Committee (IACUC) of SUNY Upstate Medical University (protocol #443) and were conducted in accordance with institutional and federal guidelines

**Author contributions:** FM, HX, AM, MSH, SM, RT, MM, and TD performed experiments, LC, analysis histological analysis JMS, Provided CAT-Tg mice. MK designed experiments, analyzed the data, and wrote the manuscript provided reagents.

**Funding Support**

This work is the result of NIH funding, in whole or in part, and is subject to the NIH Public Access Policy. Through acceptance of this federal funding, the NIH has been given a right to make the work publicly available in PubMed Central.

- Upstate Medical University Cancer Center PTA 1184369 To MK
- Carol Baldwin Breast Cancer Research. PTA is 1192750 to MK
- NIH institution of aging grant # 1R21AG098389 to MK
- Paige Butterfly Run Fund Grant #33875 to MK

This research was supported in part by the Intramural Research Program of the NIH. Contributions by NIH authors constitute Works of the United States Government. The findings and conclusions presented are those of the authors and do not necessarily reflect the official views of the NIH or the HHS. To Dr. Jyoti Misra Sen (National Institute on Aging, NIH).

**Acknowledgements:** We thank all members of the Karimi for helpful discussions.

To whom correspondence should be addressed:
Mobin Karimi M.D, Ph.D.
Assistant Professor of Immunology and Microbiology
SUNY Upstate Medical University,
766 Irving Ave Weiskotten Hall Suite 2281,
Syracuse, NY 13210
Office Phone: 315-464-2344
Laboratory Phone: 315-464-7652
Email: karimim@upstate.edu

# References


1. Barile LA, Jara LJ, Medina-Rodriguez F, Garcia-Figueroa JL, and Miranda-Limon JM. Pulmonary hemorrhage in systemic lupus erythematosus. *Lupus.* 1997;6(5):445-8.
2. Al-Adhoubi NK, and Bystrom J. Systemic lupus erythematosus and diffuse alveolar hemorrhage, etiology and novel treatment strategies. *Lupus.* 2020;29(4):355-63.
3. Morales-Nebreda L, Alakija O, Ferguson KT, and Singer BD. Systemic lupus erythematosus-associated diffuse alveolar hemorrhage: A case report and review of the literature. *Clin Pulm Med.* 2018;25(5):166-9.
4. Ramaswami A, Kandaswamy T, Rajendran T, Aung H, Jacob CK, Zinna HS, et al. Goodpasture's syndrome with positive C-ANCA and normal renal function: a case report. *J Med Case Rep.* 2008;2:223.
5. Yendamuri S. Massive Airway Hemorrhage. *Thorac Surg Clin.* 2015;25(3):255-60.
6. Chorti A, Bontinis V, Bontinis A, Alifieris CE, Chatziantoniou G, Karlafti E, et al. A systematic review meta-analysis and meta-regression on the implications of an aberrant right hepatic artery in patients undergoing pancreaticoduodenectomy for the treatment of malignant disease. *Minerva Surg.* 2024;79(1):82-91.
7. Reddy R, and Ln S. A Tale of Immune Fragility: Severe Mycoplasma pneumoniae Infection With Mixed Autoimmune Hemolytic Anemia in Selective IgM Deficiency Disorder. *Cureus.* 2025;17(9):e93550.
8. Hus A, Wislowska M, and Bonek K. Granulomatosis with Polyangiitis (GPA) in a Polish Tertiary Centre (2010-2025): Sex-Stratified Phenotypes, Serology, and Evolving Treatment Patterns. *J Clin Med.* 2025;14(21).
9. Wang MH, Liu J, Li SL, Zheng MZ, Qu RY, and Xiang M. Amphiregulin: a potential therapeutic target for tissue fibrosis. *Trends Pharmacol Sci.* 2025;46(9):877-90.
10. Ehnold LI, Melderis S, Hagenstein J, Warkotsch MT, Laas V, Feindt FC, et al. Treg derived Amphiregulin protects from murine lupus nephritis via tissue reparative effects. *Sci Rep.* 2025;15(1):7776.
11. Zaiss DMW, Gause WC, Osborne LC, and Artis D. Emerging functions of amphiregulin in orchestrating immunity, inflammation, and tissue repair. *Immunity.* 2015;42(2):216-26.
12. Wang X, Hong Y, Zou J, Zhu B, Jiang C, Lu L, et al. The role of BATF in immune cell differentiation and autoimmune diseases. *Biomark Res.* 2025;13(1):22.
13. Karwacz K, Miraldi ER, Pokrovskii M, Madi A, Yosef N, Wortman I, et al. Critical role of IRF1 and BATF in forming chromatin landscape during type 1 regulatory cell differentiation. *Nat Immunol.* 2017;18(4):412-21.
14. Qiu H, Wu H, Chan V, Lau CS, and Lu Q. Transcriptional and epigenetic regulation of follicular T-helper cells and their role in autoimmunity. *Autoimmunity.* 2017;50(2):71-81.
15. Khatun A, Wu X, Qi F, Gai K, Kharel A, Kudek MR, et al. BATF is Required for Treg Homeostasis and Stability to Prevent Autoimmune Pathology. *Adv Sci (Weinh).* 2023;10(28):e2206692.

16. Latasa MU, Salis F, Urtasun R, Garcia-Irigoyen O, Elizalde M, Uriarte I, et al. Regulation of amphiregulin gene expression by beta-catenin signaling in human hepatocellular carcinoma cells: a novel crosstalk between FGF19 and the EGFR system. *PLoS One.* 2012;7(12):e52711.
17. Lin HH, Peng YJ, Tsai MJ, Wu YY, Tsai TN, Huang HH, et al. Upregulation of amphiregulin by retinoic acid and Wnt signalling promotes liver cancer cell proliferation. *J Cell Physiol.* 2020;235(2):1689-99.
18. Liu J, Xiao Q, Xiao J, Niu C, Li Y, Zhang X, et al. Wnt/beta-catenin signalling: function, biological mechanisms, and therapeutic opportunities. *Signal Transduct Target Ther.* 2022;7(1):3.
19. Sampietro J, Dahlberg CL, Cho US, Hinds TR, Kimelman D, and Xu W. Crystal structure of a beta-catenin/BCL9/Tcf4 complex. *Mol Cell.* 2006;24(2):293-300.
20. Pai SG, Carneiro BA, Mota JM, Costa R, Leite CA, Barroso-Sousa R, et al. Wnt/beta-catenin pathway: modulating anticancer immune response. *J Hematol Oncol.* 2017;10(1):101.
21. Tsao HW, Kaminski J, Kurachi M, Barnitz RA, DiIorio MA, LaFleur MW, et al. Batf-mediated epigenetic control of effector CD8(+) T cell differentiation. *Sci Immunol.* 2022;7(68):eabi4919.
22. Wu X, Kasmani MY, Zheng S, Khatun A, Chen Y, Winkler W, et al. BATF promotes group 2 innate lymphoid cell-mediated lung tissue protection during acute respiratory virus infection. *Sci Immunol.* 2022;7(67):eabc9934.
23. Zaiss DM, van Loosdregt J, Gorlani A, Bekker CP, Grone A, Sibilia M, et al. Amphiregulin enhances regulatory T cell-suppressive function via the epidermal growth factor receptor. *Immunity.* 2013;38(2):275-84.
24. Mammadli M, Harris R, Mahmudlu S, Verma A, May A, Dhawan R, et al. Wnt/β-catenin regulates alloreactive T cells for the treatment of hematological malignancies. *bioRxiv.* 2021:2021.04.12.439538.
25. Berga-Bolanos R, Sharma A, Steinke FC, Pyaram K, Kim YH, Sultana DA, et al. beta-Catenin is required for the differentiation of iNKT2 and iNKT17 cells that augment IL-25-dependent lung inflammation. *BMC Immunol.* 2015;16:62.
26. Berga-Bolanos R, Zhu WS, Steinke FC, Xue HH, and Sen JM. Cell-autonomous requirement for TCF1 and LEF1 in the development of Natural Killer T cells. *Mol Immunol.* 2015;68(2 Pt B):484-9.
27. Ma J, Wang R, Fang X, and Sun Z. beta-catenin/TCF-1 pathway in T cell development and differentiation. *J Neuroimmune Pharmacol.* 2012;7(4):750-62.
28. Wang R, Xie H, Huang Z, Ma J, Fang X, Ding Y, et al. T cell factor 1 regulates thymocyte survival via a RORgammat-dependent pathway. *J Immunol.* 2011;187(11):5964-73.
29. Mulroy T, Xu Y, and Sen JM. beta-Catenin expression enhances generation of mature thymocytes. *Int Immunol.* 2003;15(12):1485-94.
30. Yu Q, Xu M, and Sen JM. Beta-catenin expression enhances IL-7 receptor signaling in thymocytes during positive selection. *J Immunol.* 2007;179(1):126-31.
31. Harris R, Mammadli M, Hiner S, Suo L, Yang Q, Sen JM, et al. TCF-1 regulates NKG2D expression on CD8 T cells during anti-tumor responses. *Cancer Immunol Immunother.* 2022.

32. Spear TT, Wang Y, Smith TW, Jr., Simms PE, Garrett-Mayer E, Hellman LM, et al. Altered Peptide Ligands Impact the Diversity of Polyfunctional Phenotypes in T Cell Receptor Gene-Modified T Cells. *Mol Ther.* 2018;26(4):996-1007.
33. Tantalo DG, Oliver AJ, von Scheidt B, Harrison AJ, Mueller SN, Kershaw MH, et al. Understanding T cell phenotype for the design of effective chimeric antigen receptor T cell therapies. *J Immunother Cancer.* 2021;9(5).
34. Yang J, Chen Y, Jing Y, Green MR, and Han L. Advancing CAR T cell therapy through the use of multidimensional omics data. *Nat Rev Clin Oncol.* 2023;20(4):211-28.
35. Ren H, Ma J, and Wang J. Correlation between apparent diffusion coefficient and Ki-67 in different pathological types of lung cancer. *Transl Cancer Res.* 2021;10(12):5364-71.
36. Mammadli M, Harris R, Suo L, May A, Gentile T, Waickman AT, et al. Interleukin-2-inducible T-cell kinase (Itk) signaling regulates potent noncanonical regulatory T cells. *Clinical and Translational Medicine.* 2021;11(12):e625.
37. Harris R, Mammadli M, Hiner S, Suo L, Yang Q, Sen JM, et al. TCF-1 regulates NKG2D expression on CD8 T cells during anti-tumor responses. *Cancer Immunol Immunother.* 2023;72(6):1581-601.
38. Liu JY, Qiao YL, Jiao WE, Tao ZZ, Xu S, and Chen SM. Changes in Circulating CD44+CD62L- Treg Subsets and CD44-CD62L+ Treg Subsets Reflect the Clinical Status of Patients with Allergic Rhinitis. *Int Arch Allergy Immunol.* 2025;186(2):120-32.
39. Kawabe T, and Sher A. Memory-phenotype CD4+ T cells: a naturally arising T lymphocyte population possessing innate immune function. *Int Immunol.* 2022;34(4):189-96.
40. Tian Y, Cox MA, Kahan SM, Ingram JT, Bakshi RK, and Zajac AJ. A Context-Dependent Role for IL-21 in Modulating the Differentiation, Distribution, and Abundance of Effector and Memory CD8 T Cell Subsets. *J Immunol.* 2016;196(5):2153-66.
41. Martin MD, Kim MT, Shan Q, Sompallae R, Xue HH, Harty JT, et al. Phenotypic and Functional Alterations in Circulating Memory CD8 T Cells with Time after Primary Infection. *PLoS Pathog.* 2015;11(10):e1005219.
42. Mammadli M, Harris R, Mahmudlu S, Verma A, May A, Dhawan R, et al. Human Wnt/beta-Catenin Regulates Alloimmune Signaling during Allogeneic Transplantation. *Cancers (Basel).* 2021;13(15).
43. Mammadli M, Huang W, Harris R, Sultana A, Cheng Y, Tong W, et al. Targeting Interleukin-2-Inducible T-Cell Kinase (ITK) Differentiates GVL and GVHD in Allo-HSCT. *Front Immunol.* 2020;11:593863.
44. Mammadli M, Huang W, Harris R, Xiong H, Weeks S, May A, et al. Targeting SLP76:ITK interaction separates GVHD from GVL in allo-HSCT. *iScience.* 2021;24(4):102286.
45. Joshi NS, Cui W, Chandele A, Lee HK, Urso DR, Hagman J, et al. Inflammation directs memory precursor and short-lived effector CD8(+) T cell fates via the graded expression of T-bet transcription factor. *Immunity.* 2007;27(2):281-95.
46. Takemoto N, Intlekofer AM, Northrup JT, Wherry EJ, and Reiner SL. Cutting Edge: IL-12 inversely regulates T-bet and eomesodermin expression during pathogen-induced CD8+ T cell differentiation. *J Immunol.* 2006;177(11):7515-9.
47. Sun L, Ma K, Wang H, Xiao F, Gao Y, Zhang W, et al. JAK1-STAT1-STAT3, a key pathway promoting proliferation and preventing premature differentiation of myoblasts. *J Cell Biol.* 2007;179(1):129-38.

48. Hu Q, Bian Q, Rong D, Wang L, Song J, Huang HS, et al. JAK/STAT pathway: Extracellular signals, diseases, immunity, and therapeutic regimens. *Front Bioeng Biotechnol.* 2023;11:1110765.
49. Han S, Zhuang H, Shumyak S, Wu J, Xie C, Li H, et al. Liver X Receptor Agonist Therapy Prevents Diffuse Alveolar Hemorrhage in Murine Lupus by Repolarizing Macrophages. *Front Immunol.* 2018;9:135.
50. Zhuang H, Han S, Lee PY, Khaybullin R, Shumyak S, Lu L, et al. Pathogenesis of Diffuse Alveolar Hemorrhage in Murine Lupus. *Arthritis Rheumatol.* 2017;69(6):1280-93.
51. Lee MH, Menezes TCF, Reisz JA, Cendali FI, Ferreira EVM, Ota-Arakaki JS, et al. Physiologic relevance of the transpulmonary metabolome in connective tissue disease-associated pulmonary vascular disease. *JCI Insight.* 2025;10(9).
52. Fang 方璞 P, Li 李欣源 X, Shan 单慧敏 H, Saredy JJ, Cueto R, Xia 夏继祥 J, et al. Ly6C(+) Inflammatory Monocyte Differentiation Partially Mediates Hyperhomocysteinemia-Induced Vascular Dysfunction in Type 2 Diabetic db/db Mice. *Arterioscler Thromb Vasc Biol.* 2019;39(10):2097-119.
53. Flynn MC, Kraakman MJ, Tikellis C, Lee MKS, Hanssen NMJ, Kammoun HL, et al. Transient Intermittent Hyperglycemia Accelerates Atherosclerosis by Promoting Myelopoiesis. *Circ Res.* 2020;127(7):877-92.
54. Yang P, Liu L, Sun L, Fang P, Snyder N, Saredy J, et al. Immunological Feature and Transcriptional Signaling of Ly6C Monocyte Subsets From Transcriptome Analysis in Control and Hyperhomocysteinemic Mice. *Front Immunol.* 2021;12:632333.
55. Boyle N, O'Callaghan M, Ataya A, Gupta N, Keane MP, Murphy DJ, et al. Pulmonary renal syndrome: a clinical review. *Breathe (Sheff).* 2022;18(4):220208.
56. Beckmann N, Sutton JM, Hoehn RS, Jernigan PL, Friend LA, Johanningman TA, et al. IFNgamma and TNFalpha mediate CCL22/MDC production in alveolar macrophages after hemorrhage and resuscitation. *Am J Physiol Lung Cell Mol Physiol.* 2020;318(5):L864-L72.
57. Takahara M, Aoyama-Ishikawa M, Shuno K, Yamauhi C, Miyoshi M, Maeshige N, et al. Role of endogenous IL-18 in the lung during endotoxin-induced systemic inflammation. *Acute Med Surg.* 2014;1(1):23-30.
58. Smith S, Wu PW, Seo JJ, Fernando T, Jin M, Contreras J, et al. IL-16/miR-125a axis controls neutrophil recruitment in pristane-induced lung inflammation. *JCI Insight.* 2018;3(15).
59. Ding Q, Liu G, Zeng Y, Zhu J, Liu Z, Jiang J, et al. Glycogen synthase kinase-3beta inhibitor reduces LPS-induced acute lung injury in mice. *Mol Med Rep.* 2017;16(5):6715-21.
60. Ding Q, Liu GQ, Zeng YY, Zhu JJ, Liu ZY, Zhang X, et al. Role of IL-17 in LPS-induced acute lung injury: an in vivo study. *Oncotarget.* 2017;8(55):93704-11.
61. Kim SR, Kim HJ, Kim DI, Lee KB, Park HJ, Jeong JS, et al. Blockade of Interplay between IL-17A and Endoplasmic Reticulum Stress Attenuates LPS-Induced Lung Injury. *Theranostics.* 2015;5(12):1343-62.
62. Sadhu S, Dalal R, Dandotiya J, Binayke A, Singh V, Tripathy MR, et al. IL-9 aggravates SARS-CoV-2 infection and exacerbates associated airway inflammation. *Nat Commun.* 2023;14(1):4060.

63. Hylton DJ, Hoffman SM, Van Rooijen N, Tomlinson S, and Fleming SD. Macrophage-produced IL-12p70 mediates hemorrhage-induced damage in a complement-dependent manner. *Shock.* 2011;35(2):134-40.
64. Guan T, Zhou X, Zhou W, and Lin H. Regulatory T cell and macrophage crosstalk in acute lung injury: future perspectives. *Cell Death Discov.* 2023;9(1):9.
65. Chen YQ, Wang CJ, Xie K, Lei M, Chai YS, Xu F, et al. Progranulin Improves Acute Lung Injury through Regulating the Differentiation of Regulatory T Cells and Interleukin-10 Immunomodulation to Promote Macrophage Polarization. *Mediators Inflamm.* 2020;2020:9704327.
66. Jovisic M, Mambetsariev N, Singer BD, and Morales-Nebreda L. Differential roles of regulatory T cells in acute respiratory infections. *J Clin Invest.* 2023;133(14).
67. Mammadli M, Suo L, Sen JM, and Karimi M. TCF-1 negatively regulates the suppressive ability of canonical and noncanonical Tregs. *J Leukoc Biol.* 2023;113(5):489-503.
68. Mammadli M, Harris R, Suo L, May A, Gentile T, Waickman AT, et al. Interleukin-2-inducible T-cell kinase (Itk) signaling regulates potent noncanonical regulatory T cells. *Clin Transl Med.* 2021;11(12):e625.
69. Savage TM, Fortson KT, de Los Santos-Alexis K, Oliveras-Alsina A, Rouanne M, Rae SS, et al. Amphiregulin from regulatory T cells promotes liver fibrosis and insulin resistance in non-alcoholic steatohepatitis. *Immunity.* 2024;57(2):303-18 e6.
70. Li H, Fang R, Ma R, Long Y, He R, Lyu H, et al. Amphiregulin promotes activated regulatory T cell-suppressive function via the AREG/EGFR pathway in laryngeal squamous cell carcinoma. *Head Face Med.* 2024;20(1):62.
71. Wang S, Zhang Y, Wang Y, Ye P, Li J, Li H, et al. Amphiregulin Confers Regulatory T Cell Suppressive Function and Tumor Invasion via the EGFR/GSK-3beta/Foxp3 Axis. *J Biol Chem.* 2016;291(40):21085-95.
72. Hao Y, Ren Z, Yu L, Zhu G, Zhang P, Zhu J, et al. p300 arrests intervertebral disc degeneration by regulating the FOXO3/Sirt1/Wnt/beta-catenin axis. *Aging Cell.* 2022;21(8):e13677.
73. Jiang Y, Liu Y, Sun Y, Liu Y, Feng L, Duan M, et al. Sevoflurane induces microRNA-18a to delay rat neurodevelopment via suppression of the RUNX1/Wnt/beta-catenin axis. *Cell Death Discov.* 2022;8(1):404.
74. Ma Y, Chen Z, and Yu G. microRNA-139-3p Inhibits Malignant Behaviors of Laryngeal Cancer Cells via the KDM5B/SOX2 Axis and the Wnt/beta-Catenin Pathway. *Cancer Manag Res.* 2020;12:9197-209.
75. Odler B, Kronbichler A, and Szpirt WM. Does plasma exchange have a role in ANCA-associated vasculitis? Viewpoint 2: plasma exchange may be useful under some circumstances. *Rheumatology (Oxford).* 2025;64(Supplement_1):i68-i70.
76. Mormile I, Nazzaro G, Filippelli M, Della Casa F, Mormile M, de Paulis A, et al. Pulmonary Involvement in Systemic Lupus Erythematosus: A Potentially Overlooked Condition. *Biomedicines.* 2025;13(6).
77. Park MS. Diffuse alveolar hemorrhage. *Tuberc Respir Dis (Seoul).* 2013;74(4):151-62.
78. Byun MK, Kim DS, Kim YW, Chung MP, Shim JJ, Cha SI, et al. Clinical features and outcomes of idiopathic pulmonary alveolar proteinosis in Korean population. *J Korean Med Sci.* 2010;25(3):393-8.

79. Choi KH, Nam TS, Kim JT, Choi SM, Park MS, Kim BC, et al. Valproate associated diffuse alveolar hemorrhage. *Eur J Neurol.* 2011;18(8):e98-9.
80. Cifuentes-Zuniga F, Arroyo-Jousse V, Soto-Carrasco G, Casanello P, Uauy R, Krause BJ, et al. IL-10 expression in macrophages from neonates born from obese mothers is suppressed by IL-4 and LPS/INFgamma. *J Cell Physiol.* 2017;232(12):3693-701.
81. Torricelli M, Voltolini C, Bloise E, Biliotti G, Giovannelli A, De Bonis M, et al. Urocortin increases IL-4 and IL-10 secretion and reverses LPS-induced TNF-alpha release from human trophoblast primary cells. *Am J Reprod Immunol.* 2009;62(4):224-31.
82. Lei H, Schmidt-Bleek K, Dienelt A, Reinke P, and Volk HD. Regulatory T cell-mediated anti-inflammatory effects promote successful tissue repair in both indirect and direct manners. *Front Pharmacol.* 2015;6:184.
83. Delgoffe GM, Woo SR, Turnis ME, Gravano DM, Guy C, Overacre AE, et al. Stability and function of regulatory T cells is maintained by a neuropilin-1-semaphorin-4a axis. *Nature.* 2013;501(7466):252-6.
84. Overacre AE, and Vignali DA. T(reg) stability: to be or not to be. *Curr Opin Immunol.* 2016;39:39-43.
85. Caswell JL, Bassel LL, Rothenburger JL, Grone A, Sargeant JM, Beck AP, et al. Observational Study Design in Veterinary Pathology, Part 2: Methodology. *Vet Pathol.* 2018;55(6):774-85.
86. Gibson-Corley KN, Olivier AK, and Meyerholz DK. Principles for valid histopathologic scoring in research. *Vet Pathol.* 2013;50(6):1007-15.
87. Verneris MR, Karimi M, Baker J, Jayaswal A, and Negrin RS. Role of NKG2D signaling in the cytotoxicity of activated and expanded CD8+ T cells. *Blood.* 2004;103(8):3065-72.
88. Karimi M, Cao TM, Baker JA, Verneris MR, Soares L, and Negrin RS. Silencing human NKG2D, DAP10, and DAP12 reduces cytotoxicity of activated CD8+ T cells and NK cells. *J Immunol.* 2005;175(12):7819-28.
89. Chan JK, Hamilton CA, Cheung MK, Karimi M, Baker J, Gall JM, et al. Enhanced killing of primary ovarian cancer by retargeting autologous cytokine-induced killer cells with bispecific antibodies: a preclinical study. *Clin Cancer Res.* 2006;12(6):1859-67.
90. Nishimura R, Baker J, Beilhack A, Zeiser R, Olson JA, Sega EI, et al. In vivo trafficking and survival of cytokine-induced killer cells resulting in minimal GVHD with retention of antitumor activity. *Blood.* 2008;112(6):2563-74.
91. Abrahamsson AE, Geron I, Gotlib J, Dao KH, Barroga CF, Newton IG, et al. Glycogen synthase kinase 3beta missplicing contributes to leukemia stem cell generation. *Proc Natl Acad Sci U S A.* 2009;106(10):3925-9.
92. Karimi MA, Aguilar O, Zou B, Bachmann MH, Carlyle JR, Baldwin CL, et al. A truncated human NKG2D splice isoform negatively regulates NKG2D-mediated function. *J Immunol.* 2014;193(6):2764-71.
93. Karimi MA, Lee E, Bachmann MH, Salicioni AM, Behrens EM, Kambayashi T, et al. Measuring cytotoxicity by bioluminescence imaging outperforms the standard chromium-51 release assay. *PLoS One.* 2014;9(2):e89357.

94. Huang Y, Clarke F, Karimi M, Roy NH, Williamson EK, Okumura M, et al. CRK proteins selectively regulate T cell migration into inflamed tissues. *J Clin Invest.* 2015;125(3):1019-32.
95. Karimi MA, Bryson JL, Richman LP, Fesnak AD, Leichner TM, Satake A, et al. NKG2D expression by CD8+ T cells contributes to GVHD and GVT effects in a murine model of allogeneic HSCT. *Blood.* 2015;125(23):3655-63.
96. Harris R, and Karimi M. Dissecting the regulatory network of transcription factors in T cell phenotype/functioning during GVHD and GVT. *Front Immunol.* 2023;14:1194984.
97. Mammadli M, Suo L, Sen JM, and Karimi M. TCF-1 Is Required for CD4 T Cell Persistence Functions during AlloImmunity. *International Journal of Molecular Sciences.* 2023;24(5):4326.
98. Mammadli M, Suo L, Sen JM, and Karimi M. TCF-1 negatively regulates the suppressive ability of canonical and non-canonical Tregs. *Journal of Leukocyte Biology.* 2023:qiad019.
99. Bray NL, Pimentel H, Melsted P, and Pachter L. Near-optimal probabilistic RNA-seq quantification. *Nat Biotechnol.* 2016;34(5):525-7.
100. Law CW, Chen Y, Shi W, and Smyth GK. voom: Precision weights unlock linear model analysis tools for RNA-seq read counts. *Genome Biol.* 2014;15(2):R29.
101. Greene AE, Charney J, Nichols WW, and Coriell LL. Species identity of insect cell lines. *In Vitro.* 1972;7(5):313-22.
102. Reiner A, Yekutieli D, and Benjamini Y. Identifying differentially expressed genes using false discovery rate controlling procedures. *Bioinformatics.* 2003;19(3):368-75.
103. Reimand J, Kull M, Peterson H, Hansen J, and Vilo J. g:Profiler--a web-based toolset for functional profiling of gene lists from large-scale experiments. *Nucleic Acids Res.* 2007;35(Web Server issue):W193-200.
104. Yu G, Wang LG, Han Y, and He QY. clusterProfiler: an R package for comparing biological themes among gene clusters. *OMICS.* 2012;16(5):284-7.
105. Subramanian A, Tamayo P, Mootha VK, Mukherjee S, Ebert BL, Gillette MA, et al. Gene set enrichment analysis: a knowledge-based approach for interpreting genome-wide expression profiles. *Proc Natl Acad Sci U S A.* 2005;102(43):15545-50.

## Figure and Legends

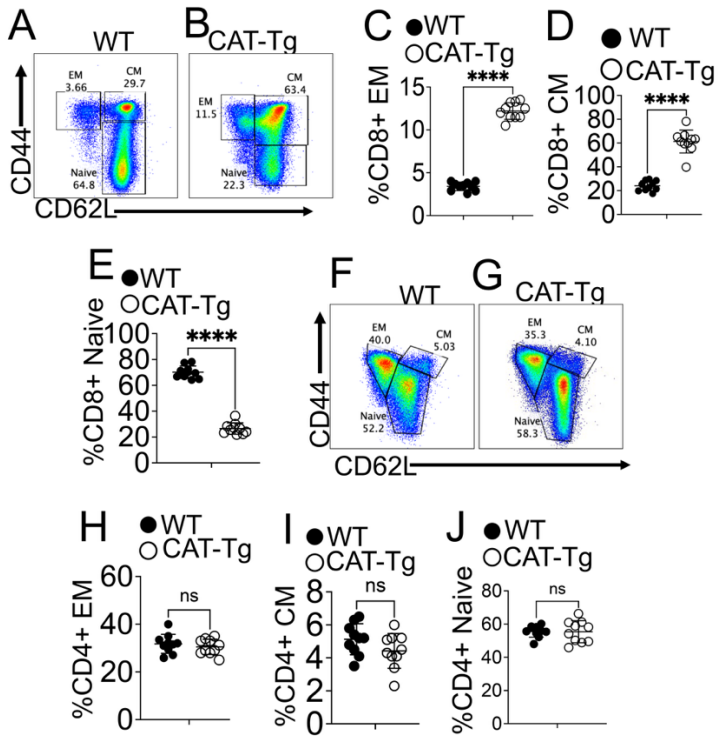


**Figure 1. β-catenin stabilization alters the CD8⁺ T cell memory phenotype:** Freshly isolated splenocytes were gated on CD3⁺ T cells and subdivided into CD4⁺ and CD8⁺ populations. Within CD8⁺ T cells, CD44 and CD62L expression was analyzed by flow cytometry (A, B). CD44⁺CD62L⁻ cells were defined as effector memory (EM), CD44⁺CD62L⁺ as central memory (CM), and CD44⁻CD62L⁺ as naïve CD8⁺ T cells. Representative flow plots from WT and CAT-Tg mice are shown, with quantification of EM, CM, and naïve CD8⁺ T cell frequencies (C–E). CD4⁺ T cells were analyzed using the same gating strategy, with representative plots and quantification of EM, CM, and naïve subsets shown (F–J). Data are presented as mean ± SEM (n = 10 mice per group; indicated in panels). Each experiment was repeated 6 times. Statistical significance was determined using the appropriate test; ****P < 0.0001.

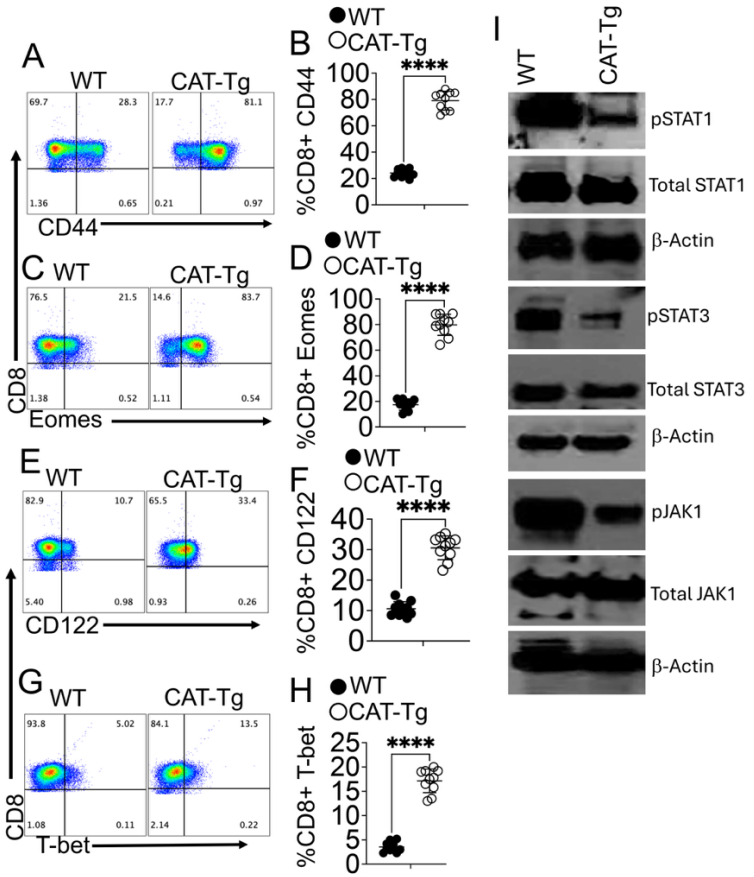


**Figure 2. CAT-Tg CD8⁺ T cells display increased activation/memory markers with reduced JAK–STAT signaling:** Freshly isolated splenocytes from WT and CAT-Tg mice were gated on $CD3^+CD8^+$ T cells. CD44 expression is shown by representative flow plots (A) with quantification (B). CD122 expression is shown by representative flow plots (E) with quantification (F). Intracellular staining for Eomes and T-bet is shown by representative flow plots (C, G) with quantification in WT and CAT-Tg mice (n = 10 per group; indicated in panels) Each experiment was repeated 6 times. For signaling analyses, $CD3^+$ T cells were MACS-purified, stimulated with anti-CD3/anti-CD28 for 3 minutes, lysed, and analyzed by immunoblotting for pSTAT1/STAT1, pSTAT3/STAT3, and JAK1, with β-actin as a loading control (I). Each experiment was repeated 3 times. Data are presented as mean ± SEM. Statistical significance was determined by two-tailed Student's *t* test; ****$P < 0.0001$.

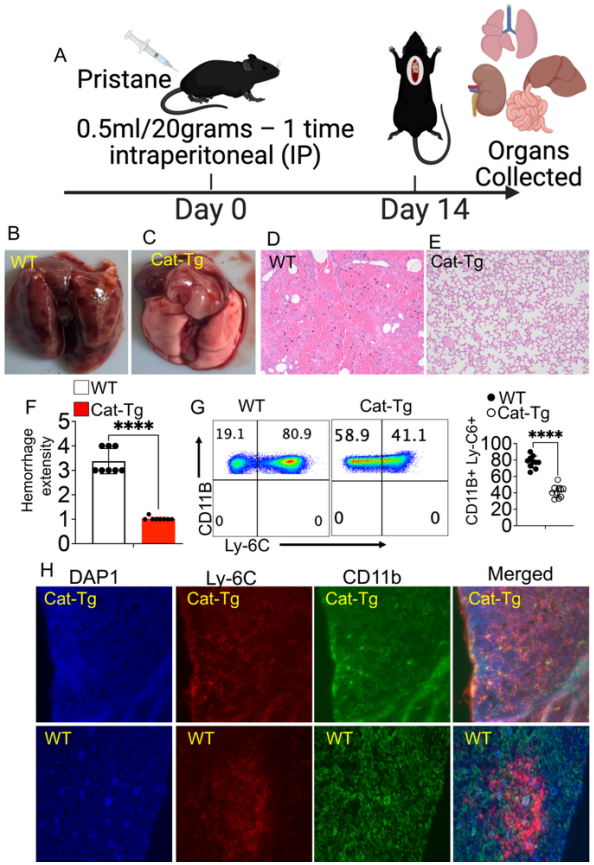


**Figure 3. β-catenin stabilization protects mice from pristane-induced alveolar hemorrhage.** (A) Experimental schematic. WT and CAT-Tg mice were injected with pristane to induce alveolar hemorrhage (AH) and euthanized on day 14 for tissue collection. (B–D) Representative gross images of lungs from WT and CAT-Tg mice. (E) Representative H&E-stained lung sections. (F) Quantification of blinded histopathologic scoring. (G) Representative flow cytometry plots and quantification of lung-infiltrating inflammatory monocytes, gated as $CD11b^{+}Ly6C^{+}$. (H) Representative immunofluorescence images of lungs at day 14 post-pristane showing DAPI (blue), Ly6C (red), and CD11b (green), with merged images. Data are presented as mean ± SEM (n = 10 mice per group). Each experiment was repeated 3 times Statistical significance was determined by two-tailed Student's *t* test; ****P < 0.0001.

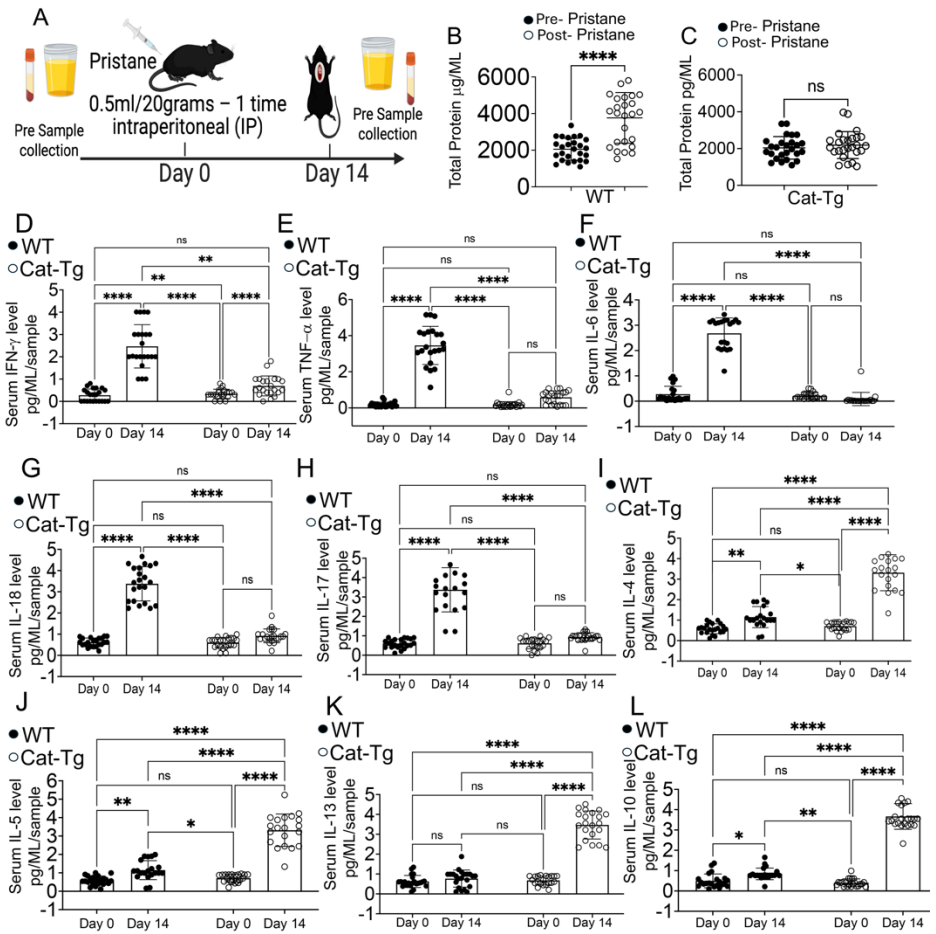


**Figure 4. β-catenin stabilization reduces proteinuria, suppresses proinflammatory cytokines, and enhances anti-inflammatory cytokines during alveolar hemorrhage.** (A) Experimental schematic. WT and CAT-Tg mice were injected with pristane to induce alveolar hemorrhage (AH). Urine and blood were collected at baseline (pre-pristane) and on day 14, followed by euthanasia. (B, C) Urinary protein was quantified by BCA assay, with comparisons between pre- and post-pristane samples in each group. (D–L) Serum cytokines were quantified by multiplex bead-based assay, including IFN-γ, TNF-α, IL-6, IL-18, IL-17, IL-4, IL-5, IL-13, and IL-10, and compared between pre- and post-pristane conditions. Data are presented as mean ± SEM; sample sizes (n = 15–25 mice per group) are indicated in panels. Each experiment was repeated 3 times. Statistical significance was determined using two-tailed Student's *t* test, one-way ANOVA, or two-way ANOVA as appropriate; **P < 0.01, ***P < 0.001, ****P < 0.0001

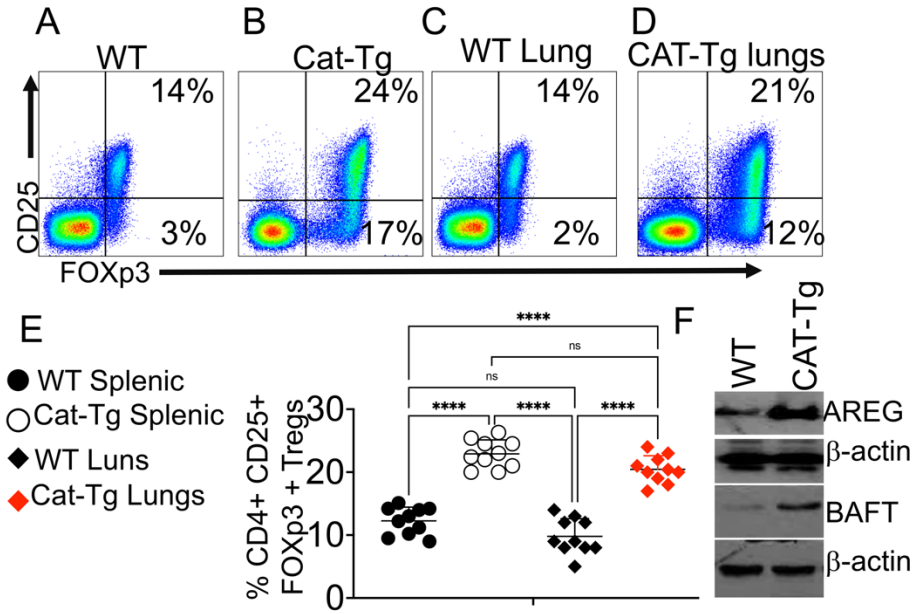


**Figure 5. β-catenin stabilization increases Tregs and enhances amphiregulin and BATF expression.** (A, B) Flow cytometry of splenocytes from WT and CAT-Tg mice. Cells were gated on $CD3^+CD4^+$ T cells and analyzed for CD25 and intracellular FOXP3 expression. (C, D) Lung leukocytes from WT and CAT-Tg mice were analyzed for Tregs using the same gating strategy ($CD3^+CD4^+CD25^+FOXP3^+$). (E) Representative flow plots and quantification of $CD4^+CD25^+FOXP3^+$ Treg frequencies. (F) $CD25^+FOXP3^+$ Tregs were FACS-sorted from lung tissue and analyzed by immunoblot for amphiregulin (AREG) and BATF, with β-actin as a loading control. Data are presented as mean ± SEM; sample sizes (n = 15–25 mice per group) are indicated in panels. Each experiment was repeated 3 times Statistical significance was determined using two-tailed Student's *t* test, one-way ANOVA, or two-way ANOVA as appropriate; $^{**}P < 0.01$, $^{***}P < 0.001$, $^{****}P < 0.0001$.

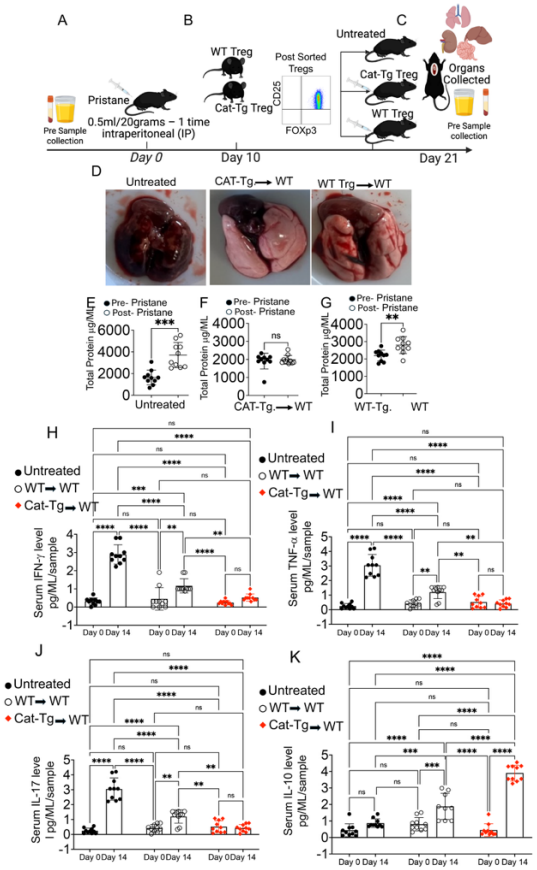


**Figure 6. Adoptive transfer of CAT-Tg Tregs rescues pristane-induced alveolar hemorrhage in vivo.** (A) Experimental schematic. WT recipient mice were assigned to three groups, and baseline urine and blood were collected. (B) $CD25^{+}FOXP3^{+}$ Tregs were isolated from WT or CAT-Tg donor mice by flow cytometry. (C) Recipients were left untreated or received $1 \times 10^{6}$ WT Tregs or $1 \times 10^{6}$ CAT-Tg Tregs by adoptive transfer. (D) Representative gross lung images from pristane-injected WT mice (untreated) and from mice receiving WT or CAT-Tg Tregs. (E) Urinary protein was quantified by BCA assay before and after pristane challenge. (F) Serum cytokines (IFN-γ, TNF-α, IL-17, and IL-10) were quantified in each group at baseline and after pristane challenge. Data are presented as mean ± SEM; sample sizes (n = 15–25 mice per group) are indicated in panels. Each experiment was repeated 3 times. Statistical significance was determined using two-tailed Student's *t* test, or two-way ANOVA as appropriate; **P < 0.01, ***P < 0.001, ****P < 0.0001.

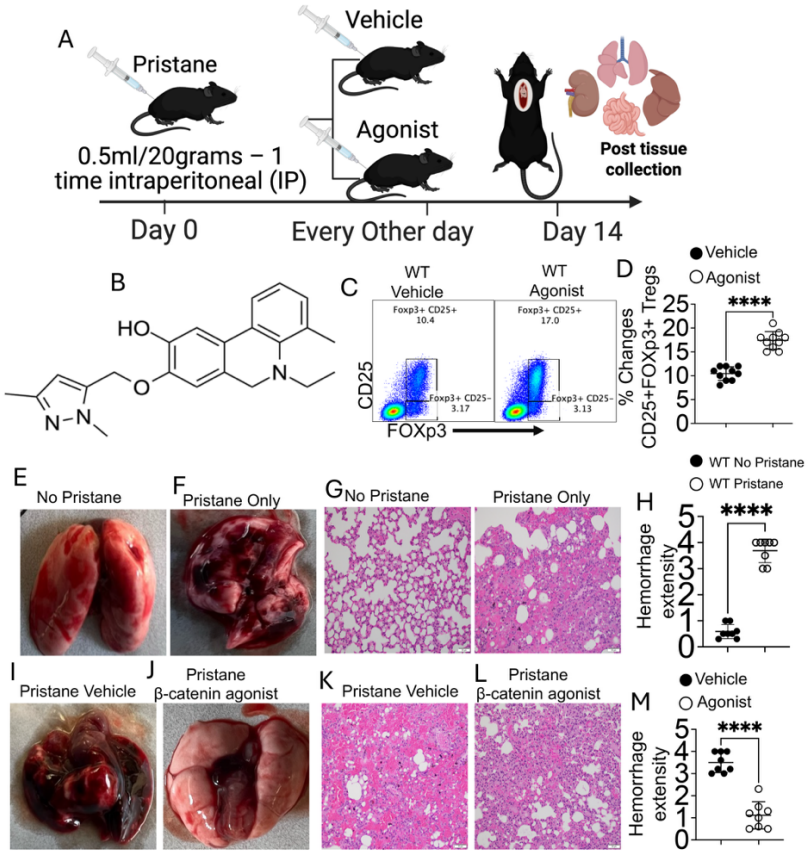


**Figure 7. β-catenin agonist treatment phenocopies genetic β-catenin stabilization and protects against pristane-induced alveolar hemorrhage.** (A) Experimental schematic. WT mice were injected with pristane to induce alveolar hemorrhage (AH) and assigned to treatment groups as indicated. (B) Chemical structure of the β-catenin agonist. (C, D) Representative flow plots and quantification of lung Tregs ($CD4^+CD25^+FOXP3^+$) in WT mice treated with vehicle or β-catenin agonist; lungs were harvested on day 14. (E, F) Gross and histologic comparison of untreated WT controls and pristane-only WT mice (no vehicle or agonist). (G, H) Representative H&E-stained lung sections and corresponding pathology scores for cohorts in (E, F). (I, J) Gross and histologic comparison of pristane-injected WT mice treated with vehicle versus β-catenin agonist (10 µg per 20 g body weight). (K–M) Representative H&E-stained lung sections and quantitative pathology scoring for cohorts in (I, J). Data are presented as mean ± SEM; sample sizes (n = 15–25 mice per group) are indicated in panels. Each experiment was repeated 3 times. Statistical significance was determined using the appropriate test; **P < 0.01, ***P < 0.001, ****P < 0.0001.

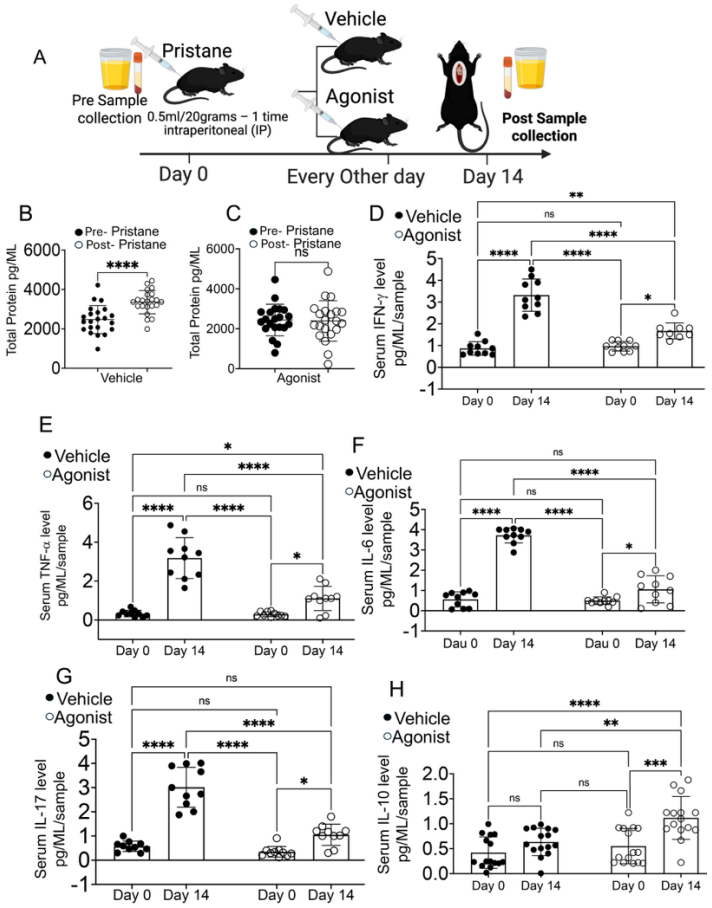


**Figure 8. β-catenin agonists reduce proteinuria and modulate cytokine responses in the AH model.** (A) Experimental schematic. Urine and blood were collected at baseline (pre-pristane). WT mice were injected with pristane to induce alveolar hemorrhage (AH) and treated with vehicle (DMSO) or β-catenin agonist (dose as indicated). On day 14, mice were euthanized and urine and serum were collected. (B–D) Urinary protein was quantified by BCA assay, with comparisons between pre- and post-pristane samples within each group. (E–H) Serum cytokines (IFN-γ, TNF-α, IL-6, IL-18, and IL-10) were quantified by multiplex bead-based assay and compared across groups and time points as indicated. Data are presented as mean ± SEM; sample sizes (n = 15–25 mice per group) are indicated in panels. Each experiment was repeated 3 times. Statistical significance was determined using two-tailed Student's *t* test, two-way ANOVA as appropriate; **P < 0.01, ***P < 0.001, ****P < 0.0001.

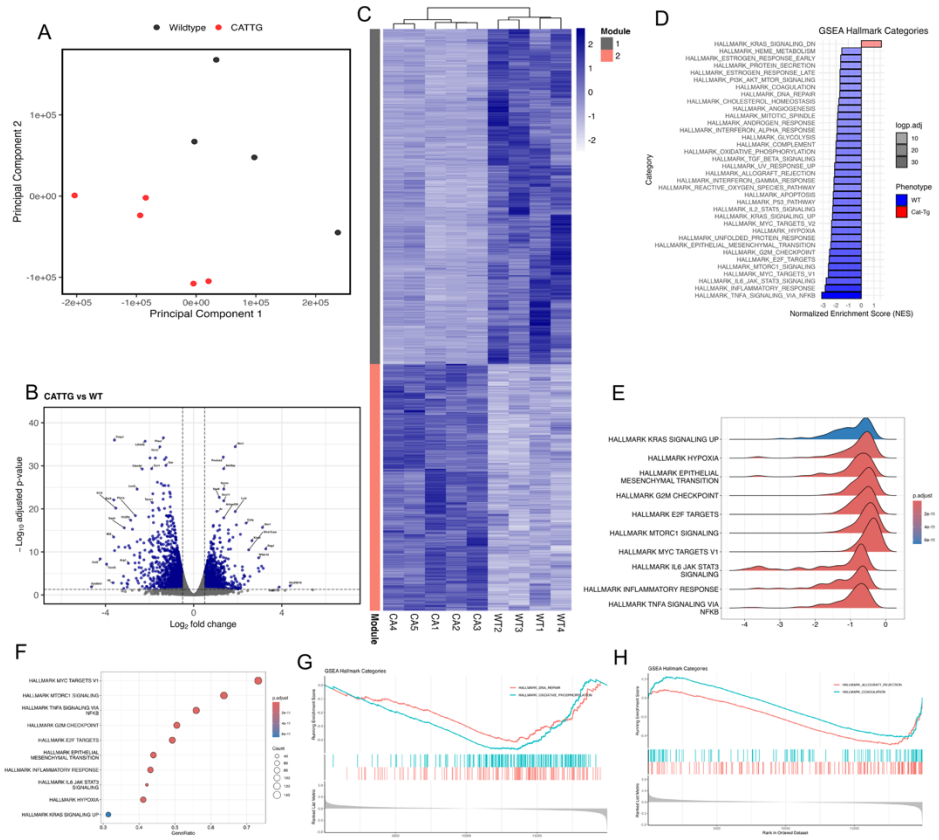


**Figure 9. β-catenin stabilization reprograms lung gene expression during pristane-induced alveolar hemorrhage.** (A) Principal component analysis (PCA) showing separation of WT and CAT-Tg lung transcriptomes at day 14 after pristane-induced AH (n = 4 per group). (B) Volcano plot of differentially expressed genes (DEGs; FDR ≤ 0.05, $|\log_2 FC| \geq 0.5$) between CAT-Tg and WT lungs; positive $\log_2 FC$ indicates higher expression in CAT-Tg. (C) Hierarchical clustering heat map of row-scaled normalized expression for DEGs across all samples (n = 4 per group). (D) Summary of Hallmark pathway enrichment by GSEA, highlighting pathways enriched in WT versus CAT-Tg lungs following AH. (E) Ridge plot showing normalized enrichment score (NES) distributions for selected Hallmark gene sets. (F) Dot plot summarizing gene ratios for selected Hallmark gene sets; dot size reflects the number of genes contributing to enrichment. (G, H) Representative GSEA enrichment plots for selected Hallmark pathways, including DNA repair and oxidative phosphorylation (G) and allograft rejection and coagulation (H).

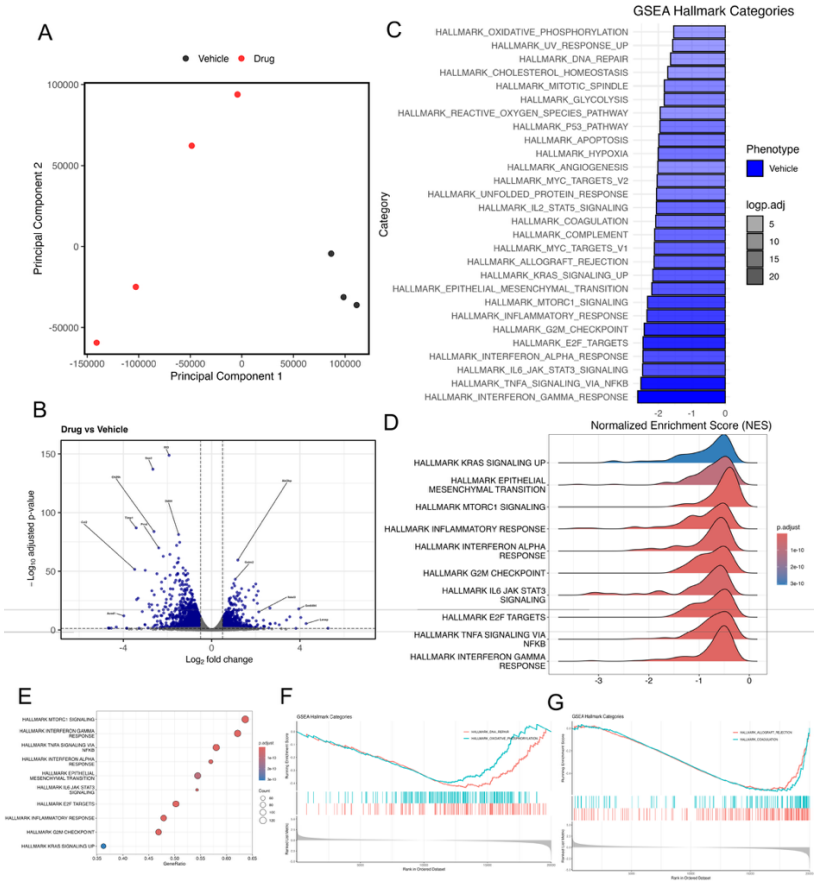


**Figure 10. β-catenin agonist treatment reprograms lung gene expression during pristane-induced alveolar hemorrhage.** (A) Principal component analysis (PCA) showing separation of vehicle- and β-catenin agonist–treated lung transcriptomes at day 14 after pristane-induced AH (n = 3 vehicle, n = 4 agonist). (B) Volcano plot of differentially expressed genes (DEGs; FDR ≤ 0.05, $|\log_2 FC| \geq 0.5$) between agonist- and vehicle-treated lungs; positive $\log_2 FC$ indicates higher expression in agonist-treated samples. (C) Summary of Hallmark pathway enrichment by GSEA, highlighting pathways enriched in vehicle versus agonist-treated lungs. (D) Ridge plot showing normalized enrichment score (NES) distributions for selected Hallmark gene sets. (E) Dot plot summarizing gene ratios for selected Hallmark gene sets; dot size reflects the number of genes contributing to enrichment. (F, G) Representative GSEA enrichment plots for selected Hallmark pathways, including DNA repair and oxidative phosphorylation (F) and allograft rejection and coagulation (G).

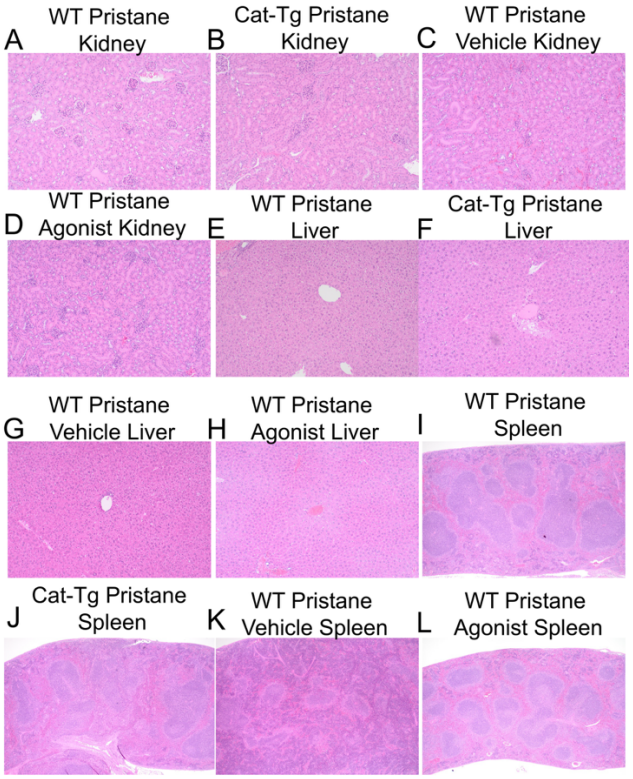


**Supplemental Figure 1. Short-term pristane exposure does not induce kidney, liver, or spleen pathology.** (A, B) Representative H&E-stained kidney sections from WT and CAT-Tg mice at day 14 after pristane injection, showing no detectable injury. (C, D) Representative H&E-stained kidney sections from pristane-injected WT mice treated with vehicle or β-catenin agonist, showing no detectable injury. (E, F) Representative H&E-stained liver sections from WT and CAT-Tg mice at day 14 after pristane injection, showing no detectable injury. (G, H) Representative H&E-stained liver sections from pristane-injected WT mice treated with vehicle or β-catenin agonist, showing no detectable injury. (I, J) Representative H&E-stained spleen sections from WT and CAT-Tg mice at day 14 after pristane injection, showing no detectable injury. (K, L) Representative H&E-stained spleen sections from pristane-injected WT mice treated with vehicle or β-catenin agonist, showing no detectable injury. Each experiment was repeated 3 times.

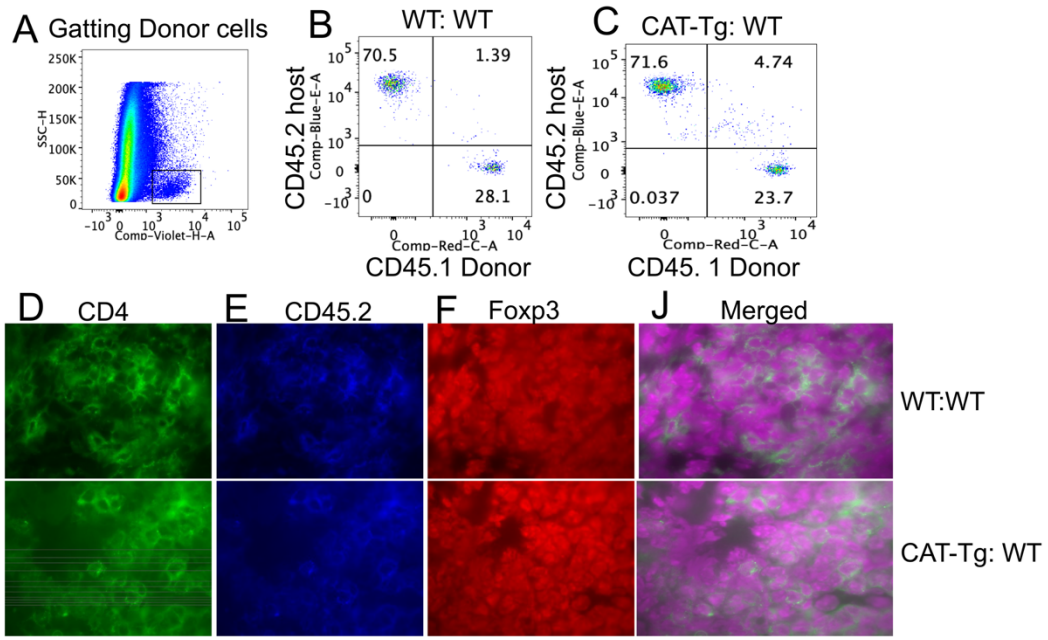


765
766 **Supplemental Figure 2. Donor Tregs persist in recipient mice and traffic to the lung.** (A–C) Congenic adoptive transfer strategy.
767 Tregs isolated from WT or CAT-Tg donor mice were transferred into congenic WT recipients on a C57BL/6 background. At day 14
768 post-transfer, spleens were harvested and $CD3^+$ T cells were analyzed by flow cytometry to distinguish donor-derived versus host-
769 derived populations based on CD45.1/CD45.2 expression, as indicated. (D–J) Immunofluorescence microscopy of lung sections
770 confirming the presence of donor Tregs in inflamed lung tissue. Sections were stained for CD4, the donor congenic marker (CD45.1 or
771 CD45.2, as indicated), and FOXP3, with merged images demonstrating colocalization; nuclei were counterstained with DAPI. Each
772 experiment was repeated 3 times.
773
774
775
776
777
778
779
780
781

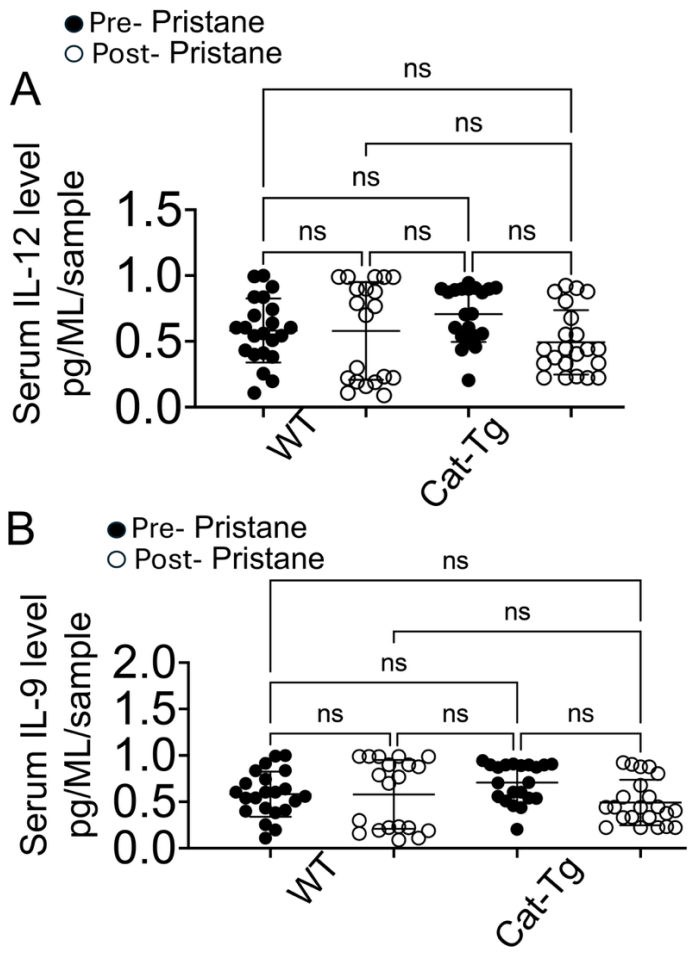


**Supplemental Figure 3. β-catenin stabilization does not alter IL-12 or IL-9 during alveolar hemorrhage.** (A, B) Serum IL-12 and IL-9 levels were quantified at baseline (pre-pristane) and after pristane-induced AH in WT, CAT-Tg, and β-catenin cKO mice using a multiplex bead-based immunoassay (LEGENDplex™, BioLegend). Data are presented as mean ± SEM; sample sizes (n = 15–25 mice per group) are indicated in panels. Statistical significance was determined using two-tailed Student's *t* test, one-way ANOVA, or two-way ANOVA as appropriate; NS denotes not significant. Each experiment was repeated 3 times.

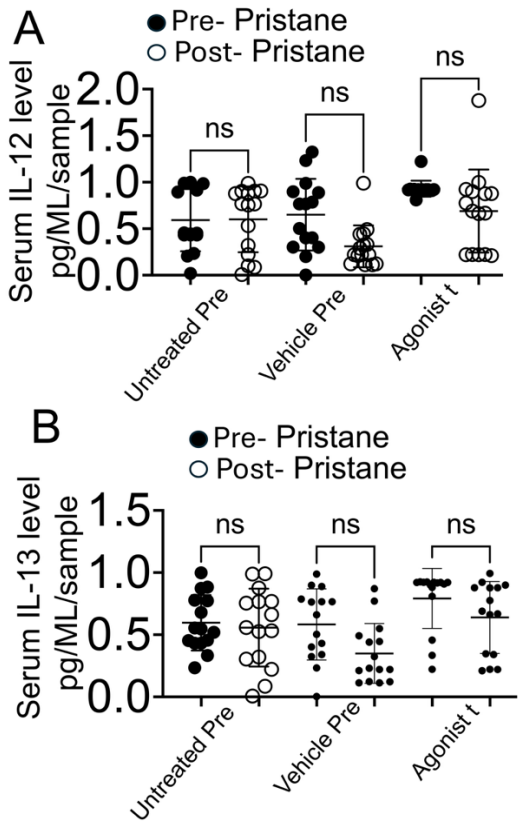


**Supplemental Figure 4. β-catenin agonist treatment does not alter IL-12 or IL-13 during AH.** (A, B) Serum IL-12 and IL-13 levels were quantified at baseline (pre-pristane) and after pristane-induced AH in WT mice treated with vehicle or β-catenin agonist using a multiplex bead-based immunoassay (LEGENDplex™, BioLegend). Data are presented as mean ± SEM; sample sizes (n = 15–25 mice per group) are indicated in panels. Statistical significance was determined using two-tailed Student's *t* test, one-way ANOVA, or two-way ANOVA as appropriate; NS denotes not significant. Each experiment was repeated 3 times.